bioRxiv preprint doi: https://doi.org/10.1101/629139; this version posted May 7, 2019. The copyright holder for this preprint (which was not certified by peer review) is the author/funder, who has granted bioRxiv a license to display the preprint in perpetuity. It is made available under aCC-BY-NC 4.0 International license.

Research Article

An *in vivo* inflammatory loop potentiates KRAS blockade

Kristina A.M. Arendt[1,*], Giannoula Ntaliarda[2,*], Vasileios Armenis[2], Danai Kati[2], Christin Henning[1], Georgia A. Giotopoulou[1,2], Mario A.A. Pepe[1], Laura V. Klotz[1], Anne-Sophie Lamort[1], Rudolf A. Hatz[3], Sebastian Kobold[4], and Georgios T. Stathopoulos[1,2,*].

[1] Comprehensive Pneumology Center (CPC) and Institute for Lung Biology and Disease (iLBD); University Hospital, Ludwig-Maximilians University and Helmholtz Zentrum München; Munich, Bavaria, 81377, Germany; Member of the German Center for Lung Research (DZL).

[2] Laboratory for Molecular Respiratory Carcinogenesis, Department of Physiology, Faculty of Medicine; University of Patras; Rio, Achaia, 26504, Greece.

[3] Center for Thoracic Surgery, Clinic for General, Visceral, Transplantation, Vascular, and Thoracic Surgery; University Hospital, Ludwig-Maximilians-Universität, 81377 Munich, Germany; Asklepios Fachkliniken München-Gauting, Gauting, Germany. Member of the German Center for Lung Research (DZL).

[4] Center of Integrated Protein Science Munich (CIPS-M) and Division of Clinical Pharmacology, Department of Medicine IV, Klinikum der Universität München; Lindwurmstraße 2a, 80337 Munich, Germany; Member of the German Center for Lung Research (DZL).

Running title: In vivo-restricted KRAS dependence.
Key words: Deltarasin; IL-1β; KRAS; inflammation; lung cancer.
Financial support: European Research Council 2010 Starting Independent Investigator and 2015 Proof of Concept Grants (260524 and 679345, respectively, to GTS).
***Corresponding authors:** Georgios T. Stathopoulos, MD PhD (stathopoulos@helmholtz-muenchen.de, gstathop@upatras.gr), Kristina Arendt (kristina.arendt@helmholtz-muenchen.de, kamarendt@hotmail.de), and Giannoula Ntaliarda (ntaliarda@upatras.gr); Lung Carcinogenesis Group, Comprehensive Pneumology Center (CPC) and Institute for Lung Biology and Disease (iLBD), Max-Lebsche-Platz 31, 81377 Munich, Germany; Phone: +49 (89) 3187 4846; Fax: +49 (89) 3187 4661; and Laboratory for Molecular Respiratory Carcinogenesis, Department of Physiology, Faculty of Medicine, University of Patras; Basic Biomedical Sciences Building, 2nd Floor, Room B40, 1 Asklepiou Str., University Campus, 26504 Rio, Greece; Phone: +30-2610-969154; Fax: +30-2610-969176.
Conflict of interest statement: The authors declare no potential conflicts of interest.
Word count: 6000
Total number of Figures/Tables: 7

bioRxiv preprint doi: https://doi.org/10.1101/629139; this version posted May 7, 2019. The copyright holder for this preprint (which was not certified by peer review) is the author/funder, who has granted bioRxiv a license to display the preprint in perpetuity. It is made available under aCC-BY-NC 4.0 International license.

ABSTRACT

KRAS inhibitors perform inferior to other targeted drugs *in vitro* and fail clinical trials. To investigate a possible reason for this, we treated human and murine tumor cells with KRAS inhibitors deltarasin (targeting phosphodiesterase-δ), cysmethynil (targeting isoprenylcysteine carboxylmethyltransferase), and AA12 (targeting $KRAS^{G12C}$), and silenced/overexpressed mutant KRAS using custom-designed vectors. We show that *KRAS*-mutant tumor cells exclusively respond to KRAS blockade *in vivo*, because the oncogene co-opts host myeloid cells via a C-C-motif chemokine ligand 2/interleukin-1β-mediated signaling loop for sustained tumorigenicity. Indeed, *KRAS*-mutant tumors did not respond to deltarasin in *Ccr2* and *Il1b* gene-deficient mice, but were deltarasin-sensitive in wild-type and *Ccr2*-deficient mice adoptively transplanted with wild-type murine bone marrow. A KRAS-dependent pro-inflammatory transcriptome was prominent in human cancers with high *KRAS* mutation prevalence and predicted poor survival. Our findings support that *in vitro* cellular systems are suboptimal for anti-KRAS drug screens since the latter drugs function to suppress interleukin-1 receptor 1 expression and myeloid IL-1β-delivered pro-growth effects *in vivo*. Moreover the findings support that interleukin-1β blockade might be suitable for the therapy of *KRAS*-mutant cancers.

bioRxiv preprint doi: https://doi.org/10.1101/629139; this version posted May 7, 2019. The copyright holder for this preprint (which was not certified by peer review) is the author/funder, who has granted bioRxiv a license to display the preprint in perpetuity. It is made available under aCC-BY-NC 4.0 International license.

INTRODUCTION

Since its discovery, the KRAS proto-oncogene GTPase (encoded by the human *KRAS* and the murine *Kras* genes) has become the holy grail of anticancer therapy [1,2]. The KRAS oncoprotein possesses a unique molecular structure that potentiates it as a driver of multiple cancer cell hallmarks (including proliferation, migration, metastasis, angiogenesis, inflammation, and apoptosis evasion), but also renders it non-actionable due to the absence of a druggable deep pocket [2,3]. KRAS point mutations that constitutively activate GTPase function occur most frequently in codons 12, 13, and 61 and are particularly frequent in pancreatic (70%), colorectal (35%), and lung (20%) adenocarcinomas [3,4]. However, full KRAS GTPase activity and downstream signaling additionally prerequisites its integration into the cell membrane, which is facilitated by post-translational lipidation and membrane transport of KRAS by various enzymes such as farnesyltransferase (FT), geranylgeranytransferase (GGT), isoprenylcysteine carboxyl methyltransferase (ICMT), phosphodiesterase-δ (PDEδ), and others [3,5]. To this end, therapeutic attempts to inhibit KRAS lipidation by targeting FT/GGT/ICMT were recently coupled by the development of PDEδ blockers and of allosteric and covalent inhibitors of mutated $KRAS^{G12C}$ [6-9].

Despite coordinated efforts [1], anti-KRAS drug discovery is lagging behind other oncogene targets [3]. In addition to molecular structural considerations [5], the mode of KRAS oncogenic functions could be a reason for this. To this end, Janes and collaborators recently reported a discordance between the *in vitro* and the *in vivo* effects of a newly developed covalent $KRAS^{G12C}$ inhibitor [9]. This observation is relevant to other reports describing how KRAS-dependence is linked to signatures of intravital-restricted processes like inflammation and epithelial-to-

bioRxiv preprint doi: https://doi.org/10.1101/629139; this version posted May 7, 2019. The copyright holder for this preprint (which was not certified by peer review) is the author/funder, who has granted bioRxiv a license to display the preprint in perpetuity. It is made available under aCC-BY-NC 4.0 International license.

mesenchymal transition [10-12] and how pro-inflammatory properties of *KRAS* mutations potentiate malignant pleural effusions in mice [13,14].

Here we hypothesized that KRAS effects and druggability are preferentially at play *in vivo*. We tested the efficacy of three different KRAS inhibitors with divergent modes of action *in vitro* and *in vivo* using a battery of 30 natural and transduced human and murine cancer cell lines and four different methods to integrally assess tumor cell growth. We consistently show that KRAS inhibitors exert ubiquitous *in vitro* effects irrespective of cellular *KRAS* mutation status, but are specifically effective against *KRAS*-mutant tumors *in vivo*. Using transcriptome analyses of cell lines expressing endogenous or exogenous wild-type or mutant *Kras* alleles, *Ccr2* and *Il1b* gene-deficient mice, as well as adoptive bone marrow transfer, we show that mutant *Kras* establishes a proinflammatory C-C motif chemokine ligand 2 (CCL2)/interleukin-1β (IL-1β)-mediated signaling loop to host myeloid cells *in vivo*, which is required for *KRAS*-mediated tumorigenicity, but also for specific KRAS inhibitor efficacy. The *KRAS/CCL2/IL1B* transcript signature is further shown to be enriched in human tumors with higher *KRAS* mutation frequencies and to portend poor survival. Our data show that intact inflammatory tumor-to-host interactions are required for full KRAS inhibitor efficacy and imply that *in vitro* drug screens might not be optimal for KRAS inhibitor discovery.

bioRxiv preprint doi: https://doi.org/10.1101/629139; this version posted May 7, 2019. The copyright holder for this preprint (which was not certified by peer review) is the author/funder, who has granted bioRxiv a license to display the preprint in perpetuity. It is made available under aCC-BY-NC 4.0 International license.

MATERIALS AND METHODS

Cell culture

NCI-H358, NCI-H358M, NCI-H460, NCI-H520, NCI-H1299, NCI-H1944, NCI-H3122 (referred to hereafter omitting NCI), EKVX, A549, LLC, B16F10, and PANO2 cell lines were from the National Cancer Institute (Frederick, MD); MC38 cells were a gift from Dr. Timothy S. Blackwell (Vanderbilt University, Nashville, TN) and AE17 cells from Dr. YC Gary Lee (University of Western Australia, Perth, Australia) [13-15]. FULA1 (*FVB* urethane-induced lung adenocarcinoma 1) and CULA (*C57BL/6* urethane-induced lung adenocarcinoma) cell lines were isolated from the lungs of *FVB* and *C57BL/6* mice, respectively, harboring primary lung adenocarcinomas induced by urethane [13,16,17]. Human and murine cell lines were cultured, respectively, in Roswell Park Memorial Institute (RPMI)-1640 and Dulbecco's Modified Eagle Medium (DMEM), both supplemented with 10% FBS and 100 IU/mL penicillin/streptomycin, and were maintained in a humidified incubator at 37 °C with 95% air–5% CO_2. Cell lines were authenticated annually using the short tandem repeat method and were tested negative for *Mycoplasma Spp.* biannually by MycoAlert Mycoplasma Detection Kit (LONZA; Verviers, Belgium).

Drugs

Deltarasin (CAS #1440898-82-7; Tocris Bio-Techne #5424; Wiesbaden-Nordenstadt, Germany), $KRAS^{G12C}$ inhibitor 12 (AA12; CAS #1469337-95-8; Selleckchem #S7331; Houston, TX), and cysmethynil (CAS #851636-83-4; Cayman Chemicals #14745; Ann Arbor, MI) were dissolved in dimethyl sulfoxide (DMSO) to 10 mM stock concentration and stored at −80 °C. For *in vitro*

bioRxiv preprint doi: https://doi.org/10.1101/629139; this version posted May 7, 2019. The copyright holder for this preprint (which was not certified by peer review) is the author/funder, who has granted bioRxiv a license to display the preprint in perpetuity. It is made available under aCC-BY-NC 4.0 International license.

and *in vivo* experiments, drugs were further diluted in normal saline and equimolar DMSO solutions were used as control.

Cellular Assays

In vitro cell proliferation was determined using water soluble tetrazolium-1 [2-(4-iodophenyl)-3-(4-nitrophenyl)-5-(2,4-disulphophenyl)-2H-teterazolium; WST-1] assay (Bimake; Munich, Germany). For this, 3000 cells/well were plated in triplicates in 96-well plates in 5% FBS-containing media and allowed to adhere overnight, followed by treatment with different drug concentrations. WST-1 reagent was added 72 hours later according to the manufacturer's protocol and absorbance at 450 nm was measured 1-4 hours later on a TECAN Sunrise microplate reader (Männedorf, Switzerland). For colony formation assay, 300 cells were plated in triplicates in 6-well plates in 5% FBS-containing media, were treated 24 hours later with 1-2 μM deltarasin, media were replaced with drug-free media 72 hours later, and cells were incubated until ≤ 50 colonies formed. Colonies were fixed with 80% ethanol, stained with 0.5% crystal violet, counted and photographed. All cellular experiments were independently repeated at least thice.

Western Immunoblotting

Cellular protein lysates were prepared using radioimmunoprecipitation assay (RIPA) buffer containing phosphatase/protease inhibitor cocktail (Thermo Fisher, Waltham, MA), separated by SDS-PAGE, and transferred to nitrocellulose membranes according to standard protocols. Anti-total (t)-extracellular-signal regulated kinase (ERK), anti-phospho (p)-ERK, and anti-glyceraldehyde 3-phosphate dehydrogenase (GAPDH) antibodies were from Santa Cruz Biotechnology (Houston, TX)(Supplementary Table S1).

bioRxiv preprint doi: https://doi.org/10.1101/629139; this version posted May 7, 2019. The copyright holder for this preprint (which was not certified by peer review) is the author/funder, who has granted bioRxiv a license to display the preprint in perpetuity. It is made available under aCC-BY-NC 4.0 International license.

Constructs

Short-hairpin (sh) RNA-mediated *Kras*-silenced (sh*Kras*) LLC, AE17, and MC38 cells, as well as B16F10 and PANO2 cells overexpressing custom-made plasmid encoding $Kras^{G12C}$ (p$Kras^{G12C}$; Addgene #64372; GFP-KrasG12C_2B_puro) were produced as described elsewhere [13]. NCI-H3122 and EKVX cells were stably transfected with p$Kras^{G12C}$ or its homologous GFP backbone plasmid without $Kras^{G12C}$ (p*C*; Addgene #64336; Bicistronic_GFP_ires_puro) using previously established methods [13]. All plasmids were made in-house, deposited, validated, and re-purchased from Addgene (Watertown, MA). Lentiviral shRNA targeting murine *Ccl2* was purchased from Santa Cruz Biotechnology (random control shRNA sc-108080-V, GFP control shRNA sc-108084-V, murine sh*Ccl2* sc-43914-SH). For stable shRNA and plasmid transfection, 10^5 tumor cells in 6-well culture vessels were transfected with 5 μg DNA using XFect (Takara, Kusatsu, Japan) and clones were selected by puromycin (2-10 μg/mL).

Mice

FVB/NJ (*FVB*; #001800), *C57BL/6J* (*C57BL/6*; #000664), B6.129P2-$Cxcr1^{tm1Dgen/J}$ ($Cxcr1^{-/-}$; #005820) [15], B6.129S4-$Ccr2^{tm1Ifc/J}$($Ccr2^{-/-}$; #004999) [16], B6.129S2(C)-$Cxcr2^{tm1Mwm/J}$ ($Cxcr2^{+/-}$; #006848) [15], and B6(Cg)-$Rag2^{tm1.1Cgn}$/J ($Rag2^{-/-}$; #008449) mice were from the Jackson Laboratory (Bar Harbor, ME) and $Il1b^{tm1Yiw}$ mice ($Il1b^{-/-}$; MGI #2157396) [18] were a kind gift from Dr. Yoichiro Iwakura (Tokyo University of Sciences, Japan). All mice were bred at the Center for Animal Models of Disease of the University of Patras. $Ccr2^{-/-}$ mice were back-crossed to the *FVB* strain for > F12. Experimental mice were weight- (20-30 g), sex-, and age- (6-12 weeks) matched; both female and male mice were used. In these studies, 284 mice were enrolled in total. In more detail, 25 *FVB* (21 for tumor experiments and 4 as bone marrow

bioRxiv preprint doi: https://doi.org/10.1101/629139; this version posted May 7, 2019. The copyright holder for this preprint (which was not certified by peer review) is the author/funder, who has granted bioRxiv a license to display the preprint in perpetuity. It is made available under aCC-BY-NC 4.0 International license.

donors), 151 *C57BL/6* (all for tumor experiments), 15 *Cxcr1*$^{-/-}$ (all on the *C57BL/6* background for tumor experiments), 34 *Ccr2*$^{-/-}$ (12 on the *C57BL/6* and 18 on the *FVB* backgrounds for tumor experiments and 4 on the *FVB* background as bone marrow donors), 12 *Cxcr2*$^{+/-}$ (all on the *C57BL/6* background for tumor experiments), 32 *Rag2*$^{-/-}$ (all on the *C57BL/6* background for tumor experiments), and 15 *Il1b*$^{-/-}$ (all on the *C57BL/6* background for tumor experiments) mice were used.

In vivo tumor models and drug treatments

For *in vivo* injections, 10^6 cells suspended in 50 µL PBS were implanted subcutaneously (sc) in the rear flank. Tumor dimensions (length, L; width, W; depth, D) were monitored serially using calipers and tumor volume (V) was calculated as $V = \pi * L * W * D/6$. Drug treatments were initiated when tumors reached 100 mm^3 volume and consisted of daily intraperitoneal (ip) deltarasin (15 mg/Kg in 100 µL saline 1% DMSO) or 100 µL saline 1% DMSO. Animals were monitored daily for sickness and were euthanized using CO_2 when in distress or when tumors reached 2-3 cm^3 volume, whichever came first.

Microarrays, PCR, GSEA, and Kaplan-Meier analyses

Isogenic cell line doublets stably expressing sh*C* or sh*Kras* (LLC, MC38, and AE17 cells) and p*C* or p*Kras*^{G12C} (PANO2 and B16F10 cells) were generated as described elsewhere [13]. Benign samples including whole murine lungs, tracheal epithelial cells (TEC; cultured out from murine tracheas), and bone marrow-derived macrophages (BMDM; cultured from murine bone marrow by weekly incubation with 20 ng/mL M-CSF) and mast cells (BMMC; cultured from murine bone marrow by monthly incubation with 100 ng/mL IL-3 plus KITL) were prepared as described elsewhere [14, 17, 18]. Cellular RNA was isolated using Trizol (Thermo Fisher)

bioRxiv preprint doi: https://doi.org/10.1101/629139; this version posted May 7, 2019. The copyright holder for this preprint (which was not certified by peer review) is the author/funder, who has granted bioRxiv a license to display the preprint in perpetuity. It is made available under aCC-BY-NC 4.0 International license.

followed by RNAeasy column purification and genomic DNA removal (Qiagen, Hilden, Germany). One µg RNA was reverse-transcribed using oligo(dT)$_{18}$ and iScript Advanced cDNA synthesis kit for RT-qPCR (Bio-Rad Laboratories; Hercules, CA). *Il1r1/IL1R1* and *Gapdh/GAPDH* qPCR was performed using specific primers (Supplementary Table S2) and Lightcycler 480 Sybr Green I Master (Roche; Mannheim, Germany) in a Lightcycler 480 II (Roche Diagnostics). Ct values from triplicate reactions were analyzed with the $2^{-\Delta CT}$ method as detailed elsewhere [15]. mRNA abundance was determined relative to *Gapdh/GAPDH* and is given as $2^{-\Delta CT} = 2^{-(\text{Ct of } Il1r1/IL1R1)-(\text{Ct of } Gapdh/GAPDH)}$. Mouse microarrays were done as described elsewhere [13-15]. Briefly, triplicate cultures of 10^6 cells were subjected to RNA extraction as above, 5 µg of pooled total RNA were tested for RNA quality on an ABI2000 Bioanalyzer (Agilent; Santa Clara, CA), labelled, and hybridized to GeneChip Mouse Gene 2.0 ST arrays (Affymetrix; Santa Clara, CA). Analyses using Affymetrix Expression/Transcriptome Analysis Consoles consisted of normalization of all arrays together using Lowess multi-array algorithm, intensity-dependent estimation of noise for statistical analysis of differential expression, and unsupervised hierarchical clustering of microarray data and WikiPathway analysis. Murine microarray data are publicly available at the Gene Expression Omnibus (GEO) database (http://www.ncbi.nlm.nih.gov/geo/; Accession ID: GSE58190). Gene set enrichment analyses (GSEA) was done using publicly available Human Gene 1.0 ST microarray data obtained from GEO. The following datasets were used: GSE31852 with gene expression profiles of 121 biopsies from patients with lung adenocarcinoma (LADC) with *EGFR* (n = 17), *KRAS* (n = 21), or none of the two (n = 83) mutations [Biomarker-integrated Approaches of Targeted Therapy for Lung Cancer Elimination (BATTLE) trial]; GSE43458 with gene expression profiles of LADC from smokers and never-smokers (n = 40 each), as well as normal lung tissue from never-

bioRxiv preprint doi: https://doi.org/10.1101/629139; this version posted May 7, 2019. The copyright holder for this preprint (which was not certified by peer review) is the author/funder, who has granted bioRxiv a license to display the preprint in perpetuity. It is made available under aCC-BY-NC 4.0 International license.

smokers (n = 30) also from the BATTLE trial; and GSE103512 with gene expression profiles of breast (n = 65), colorectal (n = 55), and non-small-cell lung (n = 60) cancer patients from a Roche dataset. Kaplan-Meier analyses were done using KM-plotter (http://www.kmplot.com) [19]. All patients were included and overall survival and all stages/grades were set as parameters.

ELISA

Murine and human CCL2 levels of cell culture supernatants were detected using appropriate ELISA kits (Peprotech; London, UK). For sample preparation, cells were incubated with IC_{60} deltarasin for 72 hours before collecting cell-free supernatants for CCL2 measurements and whole cellular lysates for normalization of CCL2 levels to total cellular protein.

Immunofluorescence

Paraffin-embedded mouse tissue blocks were cut into 3 µm-thick sections, deparaffinized by ethanol gradient, rehydrated, and boiled in sodium citrate pH 6.0 for 10 minutes for antigen retrieval. After post-fixation and permeabilization, tissue sections were co-stained with either AlexaFluor488-conjugated mouse monoclonal anti-IL-1β antibody and rabbit polyclonal anti-CCR2 antibody or AlexaFluor488-conjugated mouse monoclonal anti-IL1R1 antibody and rabbit polyclonal anti-CCL2 antibody (Supplementary Table S2). After counterstaining with 300 nM 4',6-diamidino-2-phenylindole (DAPI), slides were evaluated on an AxioImager.M2 (Zeiss; Jena, Germany) and digital images were processed with Fiji academic software (https://fiji.sc/). Control stains were carried out with isotype controls for normal mouse IgG1/ IgG2a (Alexa Fluor® 488 conjugated; sc-3891/ sc-3890) and secondary antibody only.

Bone marrow replacement

bioRxiv preprint doi: https://doi.org/10.1101/629139; this version posted May 7, 2019. The copyright holder for this preprint (which was not certified by peer review) is the author/funder, who has granted bioRxiv a license to display the preprint in perpetuity. It is made available under aCC-BY-NC 4.0 International license.

For adoptive bone marrow transplants (BMT), bone marrow cells were flushed from both femurs and tibias of wild-type (*WT*) or *Ccr2*$^{-/-}$ mice (all back-crossed >F12 to the *FVB* background) using fully supplemented DMEM. *Ccr2*$^{-/-}$ mice (all *FVB*) received ten million intravenous (iv) bone marrow cells from *WT* or *Ccr2*$^{-/-}$ mice 12 hours after total-body irradiation (900 Rad), as described elsewhere [14,15,18]. One mouse in each experiment was not engrafted and was observed till moribund on days 5-15 post-irradiation. One month was allowed for full bone marrow reconstitution of chimeras prior to tumor cell injections.

Statistics

Sample size was calculated using G*power (http://www.gpower.hhu.de/) [20]. In specific, we set out to determine biologically (> 50%) and statistically ($\alpha = 0.05$; $\beta = 0.20$) significant differences between two unmatched independent groups with SD ~ 30% of mean using two-tailed t-tests, yielding $n = 7$/group. Hence experiments with $n = 5$ mice/group were contemplated in batches, till the achievement of probability (P) < 0.05 with $\alpha < 0.05$ or $P > 0.05$ with $\beta < 0.20$, whichever came first. Two-way ANOVA was employed to achieve further reduction. Results are given as mean ± SD. Sample size (n) refers to biological replicates. Differences between means were assessed using one-way or two-way ANOVA with Bonferroni post-tests. Fifty and 60% inhibitory concentrations ($IC_{50/60}$) were calculated using nonlinear regression, a logarithmic inhibitor-response model, unweighted least squares regression without outlier elimination and constraints, and extra sum-of-squares F-test comparisons. $P < 0.05$ was considered significant. Statistics and plots were done on Prism versions 5.0, 6.0, and 8.0 (GraphPad; San Diego, CA).

Study approval

bioRxiv preprint doi: https://doi.org/10.1101/629139; this version posted May 7, 2019. The copyright holder for this preprint (which was not certified by peer review) is the author/funder, who has granted bioRxiv a license to display the preprint in perpetuity. It is made available under aCC-BY-NC 4.0 International license.

Experiments were approved by the Veterinary Administration of the Prefecture of Western Greece (approval # 366456/1461) and by the Government of Upper Bavaria (approval # 55.2-1-54-2532-194-2016) and were conducted according to Directive 2010/63/EU (http://eurlex.europa.eu/legal-content/EN/TXT/?uri=CELEX%3A32010L0063).

bioRxiv preprint doi: https://doi.org/10.1101/629139; this version posted May 7, 2019. The copyright holder for this preprint (which was not certified by peer review) is the author/funder, who has granted bioRxiv a license to display the preprint in perpetuity. It is made available under aCC-BY-NC 4.0 International license.

RESULTS

Mutation-independent effects of KRAS inhibitors *in vitro*

We initially investigated the cellular responses of a battery of human and murine cell lines with known *KRAS/Kras* mutation status [4,13-15] (Supplementary Figures S1A, S1B) to three preclinical KRAS inhibitors: deltarasin targeting PDEδ [7], AA12 allosterically targeting $KRAS^{G12C}$ [8], and cysmethynil targeting ICMT [6] (Figure 1A). For this, widely used assays were employed based on literature searches (Supplementary Figure S1C). Initially, IC_{50} values were calculated from WST-1 assays done after 72 hours of treatment with half-log-incremental drug concentrations. Unexpectedly, all three KRAS inhibitors showed comparable efficacy across all cell lines tested, independent of their *KRAS/Kras* mutation status (Figures 1B-1D; Supplementary Figure S2). Importantly, overall *in vitro* efficacy of all three drugs was modest, with IC_{50} values between 1-50 μM (Supplementary Tables S3-S5). A literature search revealed that this was generally true for developmental KRAS inhibitors compared with tyrosine kinase inhibitors (Supplementary Figure S1D). To extend these results, we analyzed the response of eight selected murine and human cell lines to IC_{60} concentrations of deltarasin in an *in vitro* colony formation assay. Again, deltarasin efficacy was independent of *KRAS/Kras* mutation status (Figures 1E, 1F; Supplementary Figure S3). Since KRAS activates the mitogen-activated protein kinase cascade inducing phosphorylation of ERK, we quantified t- and p-ERK relative to GAPDH in 12 murine and human cell lines treated with saline or IC_{60} deltarasin. In line with the above, deltarasin inhibited p-ERK independent from cellular *KRAS/Kras* mutation status (Figures 1G, 1H; Supplementary Figure S4). Thus, pharmacologic KRAS inhibition does not reveal KRAS-dependence *in vitro*.

bioRxiv preprint doi: https://doi.org/10.1101/629139; this version posted May 7, 2019. The copyright holder for this preprint (which was not certified by peer review) is the author/funder, who has granted bioRxiv a license to display the preprint in perpetuity. It is made available under aCC-BY-NC 4.0 International license.

Specific *in vivo* effects of deltarasin against *KRAS*-mutant tumors

To replicate these results *in vivo*, we induced sc tumors in *C57BL/6*, *FVB*, and *Rag2*$^{-/-}$ mice using six different cancer cell lines and initiated daily ip saline or deltarasin (15 mg/Kg in saline) treatments after tumor establishment (tumor volume ≥ 100 mm^3; latency ≥ 14 days post-sc injection). Interestingly, deltarasin selectively inhibited the sc growth of murine and human *KRAS*-mutant tumors, but had no effect on *KRAS-WT* tumors (Figures 2A, 2B). Moreover, forced overexpression of p*Kras*^{G12C} in *KRAS-WT* mouse and human cancer cells accelerated tumor growth and restored the response to the drug (Figure 2C). Taken together, these data show that deltarasin-mediated KRAS inhibition selectively halts the growth of *KRAS*-mutant cancer cells *in vivo*.

Genetic *KRAS* manipulation reveals contrasting *KRAS*-dependencies *in vitro* and *in vivo*

To further validate the observed *in vivo*-restricted specificity of deltarasin, we overexpressed anti-*Kras*-specific shRNA (sh*Kras*) in *Kras*-mutant parental cell lines or p*Kras*^{G12C} in *Kras-WT* parental cell lines [13]. In accord with pharmacologic KRAS inhibition, genetic *Kras* modulation did not impact the *in vitro* response of cancer cell lines to deltarasin, as determined by WST-1 IC_{50} values and ERK activation levels (Figures 3A-3E, Supplementary Figures S5, S6). In contrast to the lack of *Kras*-dependence *in vitro*, mutant *Kras* was required and sufficient for sustained tumor growth *in vivo* (Figure 3F): murine cell lines expressing sh*Kras* displayed statistically ($P < 0.001$) and biologically (50-90% inhibition) significantly decreased tumor growth compared with parental cell lines expressing sh*C*. *Vice versa*, p*Kras*^{G12C} overexpression accelerated tumor growth compared with overexpression of p*C*. Collectively, these results

bioRxiv preprint doi: https://doi.org/10.1101/629139; this version posted May 7, 2019. The copyright holder for this preprint (which was not certified by peer review) is the author/funder, who has granted bioRxiv a license to display the preprint in perpetuity. It is made available under aCC-BY-NC 4.0 International license.

support that, similar to drug-based KRAS inhibition, genetic *Kras* modulation selectively impacts tumor growth *in vivo*.

A mutant *Kras* transcriptome signature contains *Ccl2* and *Il1b*

In an effort to identify mutant-*Kras*-driven genes responsible for *in vivo* restricted KRAS-dependence, we analyzed the global transcriptomes of the parental and *Kras*-modulated murine cell lines described above and of benign samples [whole lungs, tracheal epithelial cells (TEC), and bone marrow-derived macrophages (BMDM) and mast cells (BMMC)]. Unsupervised hierarchical clustering showed an absolute segregation of benign, *Kras-WT*, and *Kras*-mutant samples by 1408 differentially expressed genes (ΔGE) using an ANOVA $P < 0.05$ threshold (Figure 4A). Paired analyses of five isogenic cancer cell line doublets with modulated *Kras* (LLC, MC38, and AE17 cells expressing sh*C* versus sh*Kras* and PANO2 and B16F10 cells expressing p*C* versus p*Kras*^{G12C}) identified another 3432 *Kras*-responsive transcripts. Out of the 170 transcripts that were present in both gene sets, 42 were both differentially represented in benign, *Kras-WT*, and *Kras*-mutant samples and responsive (ΔGE > 1.40) to *Kras* modulation, including *Kras per se* (Figure 4B, Supplementary Table S6). Interestingly, *Il1r1*, *Ccl7*, and *Ccl2* were among those genes and clustered tightly together (Figure 4C) and chemokine signaling was the pathway most significantly perturbed by *Kras* modulation on WikiPathway analysis (Figure 4D) [21]. We next translated our 42-gene murine mutant *Kras* signature to their 37 human orthologues using Orthoretriever (http://lighthouse.ucsf.edu/orthoretriever/) and ran GSEA (http://software.broadinstitute.org/gsea/index.jsp) [22]. Interestingly, our humanized mutant *KRAS* signature was enriched in only two out of the Broad Institute's 50 hallmark signatures: positively in the signature "inflammatory response" and negatively in the signature "G2M-checkpoint" (Figure 4E). Moreover, this mutant *KRAS* signature was significantly positively

bioRxiv preprint doi: https://doi.org/10.1101/629139; this version posted May 7, 2019. The copyright holder for this preprint (which was not certified by peer review) is the author/funder, who has granted bioRxiv a license to display the preprint in perpetuity. It is made available under aCC-BY-NC 4.0 International license.

enriched in *KRAS*- versus *EGFR*-mutant LADC (GSE43458) from the BATTLE trial [23, 24] (Figure 4F). In this connection, we recently reported that mutant *KRAS* drives CCL2 and Il1R1 expression to establish inflammatory feedback loops with IL-1β-secreting myeloid cells in malignant pleural effusions [13, 14, 18]. Collectively, the data further supported that *in vivo*-restricted mutant *KRAS*-dependence is mediated by proinflammatory signals to CCR2+ IL-1β-secreting host cells.

CCR2+ IL-1β-secreting myeloid cells potentiate *in vivo* KRAS-dependence

These results led us to the hypothesis that CCR2+ IL-1β-secreting myeloid cells are required for *in vivo* KRAS-dependence (Figure 5A). Indeed, numerous such cells co-expressing CCR2 and IL-1β were identified in the stromata of our experimental *KRAS*-mutant tumors by immunohistochemistry (Figure 5B). To definitively test our hypothesis, we induced flank tumors by injecting one million LLC cells ($Kras^{G12C}$) sc into syngeneic *C57BL/6* mice competent (*WT*) or deficient ($Il1b^{-/-}$, $Ccr2^{-/-}$) [16, 18] in the *Il1b* and *Ccr2* genes. Mice haplo/diplo-insufficient in the *Cxcr1* and *Cxcr2* chemokine receptor genes ($Cxcr1^{-/-}$, $Cxcr2^{+/-}$) [15] were also employed as additional controls for $Ccr2^{-/-}$ mice and daily ip saline or 15 mg/Kg deltarasin treatments were initiated when tumors reached 100 mm^3 volumes. Expectedly, deltarasin treatment statistically and biologically significantly inhibited LLC tumor growth in *WT*, $Cxcr1^{-/-}$, and $Cxcr2^{+/-}$ mice. However, deltarasin effects were diminished in $Il1b^{-/-}$ and completely abrogated in $Ccr2^{-/-}$ mice (Figure 5C). To exclude the possibility of developmental effects of knockout mice, we total-body irradiated (900 Rad) $Ccr2^{-/-}$ mice and performed adoptive BMT from *WT* or $Ccr2^{-/-}$ donors, as described previously [14, 18]. For this experiment, *WT* and $Ccr2^{-/-}$ mice back-crossed > F12 to the *FVB* strain were used together with syngeneic FULA1 cells ($Kras^{Q61R}$) to obtain results with another cell line harboring a different *Kras* mutation and a broad mutation spectrum relevant to

bioRxiv preprint doi: https://doi.org/10.1101/629139; this version posted May 7, 2019. The copyright holder for this preprint (which was not certified by peer review) is the author/funder, who has granted bioRxiv a license to display the preprint in perpetuity. It is made available under aCC-BY-NC 4.0 International license.

human *KRAS*-mutant LADC [17]. Again, daily ip saline or deltarasin treatments were started when tumors > 100 mm^3 were established. Expectedly, *Ccr2*$^{-/-}$ chimeras receiving *Ccr2*$^{-/-}$ BMT did not respond to deltarasin, but *Ccr2*$^{-/-}$ chimeras receiving *WT* BMT displayed markedly increased tumor growth as well as a statistically and biologically significant inhibition by deltarasin treatment (Figure 6A). Collectively, these results indicate that myeloid CCR2 and IL-1β are required for deltarasin efficacy against *Kras*-mutant tumors *in vivo*.

Deltarasin limits IL-1β sensing by *KRAS*-mutant tumor cells

We next interrogated the mechanism of *in vivo*-restricted deltarasin dependence. Based on the microarray-derived mutant *Kras* signature that encompassed *Ccl2* and *Il1r1* (Figure 4) and our previous reports of mutant *KRAS*-mediated transcriptional regulation of *CCL2* and *IL1R1* [13, 14], we tested whether deltarasin blocks expression of these two genes. Indeed, *KRAS*-mutant mouse and human cancer cell lines displayed markedly increased baseline *Il1r1/IL1R1* mRNA expression compared with *WT* cell lines, and significantly downregulated *Il1r1/IL1R1* transcript levels after deltarasin treatment. On the contrary, only some *KRAS*-mutant cell lines displayed increased baseline CCL2 protein secretion compared with *WT* cell lines, and CCL2 elaboration was not consistently blocked by deltarasin treatment, suggesting that deltarasin-mediated downregulation of *Il1r1/IL1R1* expression delivers the bulk of the drug's *in vivo* effects.

An inflammatory *CCL2/IL1B* signature in *KRAS*-mutant human cancers

To investigate the relevance of our findings to *KRAS*-mutant human cancers, we analyzed the average expression of *KRAS*, *CCL2*, and *IL1B* genes in public data (GSE43458) from the BATTLE trial [23, 24]. Interestingly, mean *KRAS/CCL2/IL1B* expression was statistically significantly increased in smokers' LADC (n = 40) compared with never-smokers' LADC (n =

bioRxiv preprint doi: https://doi.org/10.1101/629139; this version posted May 7, 2019. The copyright holder for this preprint (which was not certified by peer review) is the author/funder, who has granted bioRxiv a license to display the preprint in perpetuity. It is made available under aCC-BY-NC 4.0 International license.

40) and normal lung tissue samples (n = 30) (Figure 7A). Since *KRAS* mutations are more frequent in LADC of smokers [25], this finding suggested that our inflammatory signature was overrepresented in tumors with higher *KRAS* mutation frequencies. This was also true in another dataset from patients with breast, colorectal, and lung cancer (GSE103512) [26], where mean *KRAS/CCL2/IL1B* expression was significantly higher in lung and colorectal cancer, which have higher *KRAS* mutation rates [4], compared with breast cancer (Figure 7B). Finally, online Kaplan-Meier analyses (http://www.kmplot.com) [19] using lung cancer patient data were done (Figure 7C). These revealed that in patients with LADC (a tumor with high KRAS mutation frequency) high *KRAS/CCL2/IL1B* expression levels portended 93% increased odds of death regardless of smoking status. On the contrary, *KRAS/CCL2/IL1B* expression did not impact the survival of patients with squamous cell lung carcinoma (a tumor with low KRAS mutation frequency). When exclusively smokers were examined (thereby enriching the sample for *KRAS*-mutant patients), high *KRAS/CCL2/IL1B* expression levels portended 128% increased odds of death in LADC and continued to have no impact on the survival of patients with squamous cell lung carcinoma. Taken together, these data suggest that *KRAS/CCL2/IL1B* transcripts are overexpressed in human *KRAS*-mutant cancers and detrimentally affect survival. Moreover, that the proposed KRAS-driven inflammatory loop may be clinically relevant.

bioRxiv preprint doi: https://doi.org/10.1101/629139; this version posted May 7, 2019. The copyright holder for this preprint (which was not certified by peer review) is the author/funder, who has granted bioRxiv a license to display the preprint in perpetuity. It is made available under aCC-BY-NC 4.0 International license.

DISCUSSION

We hypothesized that mutant *KRAS* dependence occurs non-cell-autonomously and that KRAS inhibitor effects are delivered *in vivo*. We used 30 cancer cell lines with different *KRAS* mutations and multiple *in vitro* assays to show that both pharmacologic and genetic KRAS inhibition is selectively effective against *KRAS*-mutant murine and human tumors *in vivo*. Using isogenic cell lines with intact or compromised mutant *KRAS* signaling, we identify a novel *KRAS*-mutation-specific transcriptome signature that is surprisingly predominated by inflammatory response genes including *CCL2* and *IL1B*. We further employ several transgenic mouse strains and adoptive bone marrow transfer experiments to show that effective pharmacologic KRAS blockade *in vivo* is dependent on the presence of CCR2+ IL-1β-secreting myeloid cells in the tumor microenvironment. Finally, we show that the KRAS blocker deltarasin functions to downregulate *IL1R1* expression in *KRAS*-mutant tumor cells and that the proposed *KRAS/CCL2/IL1B* signature is enriched in human cancers with high *KRAS* mutation frequencies in which it portends a dismal prognosis. Our results imply that conventional cell-based screens for the discovery and development of novel KRAS blockers might be suboptimal, and that IL-1β inhibition may be specifically effective against KRAS-mutant cancers.

A long line of evidence supports that homotypic two-dimensional cancer cell cultures are not optimal for the study of KRAS-dependence. Singh et al. established a "RAS-dependency index" in a large panel of human lung and pancreatic cancer cell lines systematically addressing the variable *in vitro* efficacy of KRAS inhibition [10]. Project DRIVE, a comprehensive synthetic lethality screen applying > 150000 shRNAs on 7,837 genes and 398 cancer cell lines (https://oncologynibr.shinyapps.io/drive/), identified no lethal interaction partners for KRAS *in vitro*, a finding that urged the authors to state: "… the data here raise the likelihood that no single

bioRxiv preprint doi: https://doi.org/10.1101/629139; this version posted May 7, 2019. The copyright holder for this preprint (which was not certified by peer review) is the author/funder, who has granted bioRxiv a license to display the preprint in perpetuity. It is made available under aCC-BY-NC 4.0 International license.

synthetic lethal gene will be found across all KRAS mutant tumors … commonly used KRAS mutant models are not KRAS dependent, when interrogated as monolayer cell cultures … ablating KRAS dependence will need to carefully consider these findings..." [12]. Recently, Janes et al. developed ARS-1620, a new covalent G12C-specific KRAS inhibitor that is highly effective *in vivo*, but not *in vitro* [9]. The authors developed three-dimensional co-culture systems and state: "We use ARS-1620 to dissect oncogenic KRAS dependency and demonstrate that monolayer culture formats significantly underestimate KRAS dependency *in vivo*". Despite the tremendous progress contributed by the above-referenced work, the mechanism(s) of the observed in vivo-restricted KRAS-dependence remained obscure prior to this report.

To this end, multiple lines of work support the notion that the paracrine effects of KRAS and other RAS oncogenes overshadow their cell-autonomous impact. A pioneering report identified how RAS oncogenes utilize paracrine IL-8 signaling to induce angiogenesis *in vivo* [11, 27]. We determined how *KRAS*-mutant cancer cells depend on paracrine CCL2 signaling to myeloid cells including mononuclear and mast cells to induce vascular permeability and angiogenesis during malignant pleural effusion development [13, 18]. In turn, myeloid-derived IL-1β was found to selectively trigger non-canonical nuclear factor (NF)-κB activation in *KRAS*-mutant cancer cells via IL1R1 and inhibitor of NF-κB kinase α (IKKα), with the latter presenting a marked therapeutic target in mouse models of pre-metastatic and advanced lung cancer [14, 28]. Here we show how deltarasin functions to abrogate a mutant *KRAS*-initiated *in vivo* inflammatory loop of tumor-derived CCL2 and myeloid-secreted IL-1β by downregulating IL1R1 expression of *KRAS*-mutant tumor cells and thereby abolishing their receptivity to myeloid IL-1β signals. We identify CCR2+ myeloid cells that provide IL-1β to the microenvironment of *KRAS*-mutant tumors and show that they are required for mutant *KRAS* dependence *in vivo*. Data from syngeneic mouse

bioRxiv preprint doi: https://doi.org/10.1101/629139; this version posted May 7, 2019. The copyright holder for this preprint (which was not certified by peer review) is the author/funder, who has granted bioRxiv a license to display the preprint in perpetuity. It is made available under aCC-BY-NC 4.0 International license.

models of global host *Ccr2* and *Il1b* gene deficiency and of focal myeloid *Ccr2* reconstitution are further supported by human cancer xenograft experiments in *Rag2*$^{-/-}$ mice, which lack B- and T-cell function but feature intact myeloid cells [29], to collectively identify the proposed inflammatory loop that potentiates KRAS blockade.

In addition to *Kras*, *Ccl2*, and *Il1b*, a battery of other transcripts emanated within the signature of *KRAS*-mutant cancers derived from the transcriptomes of our cell lines, providing synthetic lethality candidates for *in vivo* KRAS dependency for future research. This signature includes signal transducers *Ranbp3l*, *Gpr149*, and *Rassf8*, inflammatory messengers *Ccl7*, *Cxcl1*, and *Casp3*, cell surface receptors *Pdgfra* and *Ttk*, cell cycle genes and tumor suppressors *Cdca5*, *Hist2h3c2*, *Plag1*, *Fanca*, and *Gmnn*, among others. The importance of some of these candidates is worth mentioning: *Cxcl1* was recently found to mediate the effects of KRAS-IKKα addiction during malignant pleural effusion development [14]; *Casp3* is a central effector of compensatory tumor proliferation and radiotherapy resistance [30]; and *Gmnn* was recently found to function as a tumor suppressor in lung and colon cancer [31]. Surprisingly, *Kras* mutation status imprinted the transcriptomes of our cell lines more profoundly than their tissues of origin, making them cluster together in an unsupervised fashion. Furthermore, our *KRAS*-mutation signature was enriched in human *KRAS*-mutant cancers and predicted poor survival, a fact that is further validating this gene set. Most importantly, the mutant *KRAS* signature was dominated by the inflammatory response pathway on both WikiPathways analysis and GSEA, highlighting the notion that the oncogene functions in a proinflammatory fashion.

In addition to fostering the battle to drug KRAS, the present work bears significant clinical implications by pinning CCL2 and IL-1β as key inflammatory addiction partners of mutant *KRAS*. Although targeting CCL2 with neutralizing antibodies yielded promising preclinical

bioRxiv preprint doi: https://doi.org/10.1101/629139; this version posted May 7, 2019. The copyright holder for this preprint (which was not certified by peer review) is the author/funder, who has granted bioRxiv a license to display the preprint in perpetuity. It is made available under aCC-BY-NC 4.0 International license.

results [13, 18, 32-35], clinical trials of the anti-human CCL2 antibody carlumab were hampered by limited drug efficacy and tolerability [36-38]. In contrast, targeting IL-1β with canakinumab has raised enthusiasm and holds great premise in cancer therapy. In this regard, the Canakinumab Anti-inflammatory Thrombosis Outcomes Study (CANTOS), a randomised trial of the role of IL-1β inhibition in atherosclerosis, secondarily aimed at establishing whether low (50 mg), medium (150 mg), or high (300 mg)-dose canakinumab given sc every three months might alter cancer incidence [39,40]. The results astonished, with total cancer mortality decreasing by 51% in the high-dose group, incident lung cancer decreasing by39% in the medium-dose and by 67% in the high-dose groups, and with lung cancer mortality decreasing by 77% in the high-dose canakinumab group. Although our results of diminished deltarasin efficacy with *Il1b*$^{-/-}$ mice were less impressive compared with the complete abrogation of deltarasin effects in *Ccl2*$^{-/-}$ mice, we believe that this is attributable to redundant IL-1α signaling in the former and that targeting IL-1β might be specifically effective against *KRAS*-mutant cancers [41-45]. This is plausible from CANTOS results, since canakinumab effects in decreasing lung cancer incidence and mortality were double in current than in past smokers overall and quadruple when the high-dose group was examined alone, with current smokers having higher *KRAS* mutation rates than never-smokers [4,23-25]. Our results suggest that canakinumab might be selectively effective against *KRAS*-mutant cancers and warrant a posteriori analysis of CANTOS results by *KRAS* mutation status.

In summary, we show that *KRAS*-mutant cancer cells express CCL2 and IL1R1 to initiate an inflammatory signaling loop with CCR2/IL-1β-expressing myeloid cells. Our work indicates that this crosstalk is required for KRAS-dependence and blockade, which targets IL1R1 expression. The data set a rational framework for the future development of effective KRAS inhibitors and design of clinical trials aimed at targeting IL-1β in cancer.

bioRxiv preprint doi: https://doi.org/10.1101/629139; this version posted May 7, 2019. The copyright holder for this preprint (which was not certified by peer review) is the author/funder, who has granted bioRxiv a license to display the preprint in perpetuity. It is made available under aCC-BY-NC 4.0 International license.

AUTHORS' CONTRIBUTIONS

KAMA performed in vitro experiments, transcriptome analyses, histology and microscopy, analyzed the data, and wrote the manuscript draft; GN, VA, and DK performed in vivo experiments; CH, LVK, and ASL performed in vitro experiments; GAG performed GSEA; MAAP performed pathway analysis and deposited microarray data at GEO; RAH and SK provided critical intellectual input; GTS designed, funded, and guided the study, analyzed the data, is the guarantor of the study's integrity, wrote the final version of the manuscript, and designed the final version of the figures. All authors reviewed and edited the paper and approved the final version before submission.

ACKNOWLEDGEMENTS

This work was supported by European Research Council 2010 Starting Independent Investigator and 2015 Proof of Concept Grants (260524 and 679345, to GTS), and by a European Respiratory Society 2013 Romain Pauwels Research Award (to GTS). The authors thank the University of Patras Center for Animal Models of Disease for experimental support. The authors have no financial conflict of interest.

bioRxiv preprint doi: https://doi.org/10.1101/629139; this version posted May 7, 2019. The copyright holder for this preprint (which was not certified by peer review) is the author/funder, who has granted bioRxiv a license to display the preprint in perpetuity. It is made available under aCC-BY-NC 4.0 International license.

REFERENCES

1. Esposito D, Stephen AG, Turbyville TJ, Holderfield M. New weapons to penetrate the armor: Novel reagents and assays developed at the NCI RAS Initiative to enable discovery of RAS therapeutics. Semin Cancer Biol 2019;54:174–82.

2. Downward J. Targeting RAS signalling pathways in cancer therapy. Nat Rev Cancer 2003;3:11–22.

3. Stephen AG, Esposito D, Bagni RK, McCormick F. Dragging ras back in the ring. Cancer Cell 2014;25:272–81.

4. Tate JG, Bamford S, Jubb HC, Sondka Z, Beare DM, Bindal N, et al. COSMIC: the Catalogue Of Somatic Mutations In Cancer. Nucleic Acids Res 2019;47:D941–D947.

5. Simanshu DK, Nissley DV, McCormick F. RAS Proteins and Their Regulators in Human Disease. Cell 2017;170:17–33.

6. Winter–Vann AM, Baron RA, Wong W, dela Cruz J, York JD, Gooden DM, et al. A small–molecule inhibitor of isoprenylcysteine carboxyl methyltransferase with antitumor activity in cancer cells. Proc Natl Acad Sci U S A 2005;102:4336–41.

7. Zimmermann G, Papke B, Ismail S, Vartak N, Chandra A, Hoffmann M, et al. Small molecule inhibition of the KRAS-PDEδ interaction impairs oncogenic KRAS signalling. Nature 2013;497:638–42.

8. Ostrem JM, Peters U, Sos ML, Wells JA, Shokat KM. K-Ras(G12C) inhibitors allosterically control GTP affinity and effector interactions. Nature 2013;503:548–51.

9. Janes MR, Zhang J, Li L-S, Hansen R, Peters U, Guo X, et al. Targeting KRAS Mutant Cancers with a Covalent G12C-Specific Inhibitor. Cell 2018;172:578–89.

10. Singh A, Greninger P, Rhodes D, Koopman L, Violette S, Bardeesy N, et al. A gene expression signature associated with "K-Ras addiction" reveals regulators of EMT and tumor cell survival. Cancer Cell 2009;15:489–500.

11. Sparmann A, Bar-Sagi D. Ras-induced interleukin-8 expression plays a critical role in tumor growth and angiogenesis. Cancer Cell 2004;6:447–58.

12. McDonald ER, Weck A de, Schlabach MR, Billy E, Mavrakis KJ, Hoffman GR, et al. Project DRIVE: A Compendium of Cancer Dependencies and Synthetic Lethal Relationships Uncovered by Large-Scale, Deep RNAi Screening. Cell 2017; 170: 577–592.e10.

13. Agalioti T, Giannou AD, Krontira AC, Kanellakis NI, Kati D, Vreka M, et al. Mutant KRAS promotes malignant pleural effusion formation. Nat Commun 2017;8:15205.

bioRxiv preprint doi: https://doi.org/10.1101/629139; this version posted May 7, 2019. The copyright holder for this preprint (which was not certified by peer review) is the author/funder, who has granted bioRxiv a license to display the preprint in perpetuity. It is made available under aCC-BY-NC 4.0 International license.

14. Marazioti A, Lilis I, Vreka M, Apostolopoulou H, Kalogeropoulou A, Giopanou I, et al. Myeloid-derived IL-1ß drives oncogenic KRAS-NF-kB addiction in malignant pleural effusion. Nat Commun 2018; 9:672.

15. Giannou AD, Marazioti A, Kanellakis NI, Giopanou I, Lilis I, Zazara DE, et al. NRAS destines tumor cells to the lungs. EMBO Mol Med 2017;9:672–686.

16. Giopanou I, Lilis I, Papaleonidopoulos V, Agalioti T, Kanellakis NI, Spiropoulou N, et al. Tumor–derived osteopontin isoforms cooperate with TRP53 and CCL2 to promote lung metastasis. Oncoimmunology 2017;6:e1256528.

17. Kanellakis NI, Giannou AD, Pepe MA, Agalioti T, Zazara DE, Giopanou I, et al. Tobacco chemical-induced mouse lung adenocarcinoma cell lines pin the prolactin orthologue proliferin as a lung tumour promoter. Carcinogenesis, 2019 Mar 4. pii: bgz047. doi: 10.1093/carcin/bgz047.

18. Giannou AD, Marazioti A, Spella M, Kanellakis NI, Apostolopoulou H, Psallidas I, et al. Mast cells mediate malignant pleural effusion formation. J Clin Invest 2015;125:2317–34.

19. Győrffy B, Surowiak P, Budczies J, Lánczky A. Online survival analysis software to assess the prognostic value of biomarkers using transcriptomic data in non–small–cell lung cancer. PloS One 2013;8:e82241.

20. Faul F, Erdfelder E, Lang A–G, Buchner A. G*Power 3: a flexible statistical power analysis program for the social, behavioral, and biomedical sciences. Behav Res Methods 2007;39:175–91.

21. Kelder T, van Iersel MP, Hanspers K, Kutmon M, Conklin BR, Evelo CT, Pico AR. WikiPathways: building research communities on biological pathways. Nucleic Acids Res 2012;40(Database issue):D1301-7.

22. Subramanian A, Tamayo P, Mootha VK, Mukherjee S, Ebert BL, Gillette MA, et al. Gene set enrichment analysis: a knowledge-based approach for interpreting genome-wide expression profiles. Proc Natl Acad Sci U S A 2005;102:15545-50.

23. Kim ES, Herbst RS, Wistuba II, Lee JJ, Blumenschein GR Jr, Tsao A, et al. The BATTLE trial: personalizing therapy for lung cancer. Cancer Discov 2011;1:44-53.

24. Kabbout M, Garcia MM, Fujimoto J, Liu DD, Woods D, Chow CW, Mendoza G, Momin AA, James BP, Solis L, Behrens C, Lee JJ, Wistuba II, Kadara H. ETS2 mediated tumor suppressive function and MET oncogene inhibition in human non-small cell lung cancer. Clin Cancer Res 2013;19:3383-95.

25. Campbell JD, Alexandrov A, Kim J, Wala J, Berger AH, Pedamallu CS, et al. Distinct patterns of somatic genome alterations in lung adenocarcinomas and squamous cell carcinomas. Nat Genet 2016;48:607–16.

bioRxiv preprint doi: https://doi.org/10.1101/629139; this version posted May 7, 2019. The copyright holder for this preprint (which was not certified by peer review) is the author/funder, who has granted bioRxiv a license to display the preprint in perpetuity. It is made available under aCC-BY-NC 4.0 International license.

26. Brouwer-Visser J, Cheng WY, Bauer-Mehren A, Maisel D, Lechner K, Andersson E, et al. Regulatory T-cell Genes Drive Altered Immune Microenvironment in Adult Solid Cancers and Allow for Immune Contextual Patient Subtyping. Cancer Epidemiol Biomarkers Prev 2018;27:103-12.

27. Karin M. Inflammation and cancer: the long reach of Ras. Nat Med 2005;11:20-1.

28. Vreka M, Lilis I, Papageorgopoulou M, Giotopoulou GA, Lianou M, Giopanou I, et al. IκB Kinase α Is Required for Development and Progression of KRAS-Mutant Lung Adenocarcinoma. Cancer Res 2018;78:2939-2951.

29. Hao Z, Rajewsky K. Homeostasis of peripheral B cells in the absence of B cell influx from the bone marrow. J Exp Med 2001;194:1151–64.

30. Huang Q, Li F, Liu X, Li W, Shi W, Liu FF, et al. Caspase 3-mediated stimulation of tumor cell repopulation during cancer radiotherapy. Nat Med 2011;17:860-6.

31. Champeris Tsaniras S, Villiou M, Giannou AD, Nikou S, Petropoulos M, Pateras IS, et al. Geminin ablation in vivo enhances tumorigenesis through increased genomic instability. J Pathol 2018;246:134-140.

32. Marazioti A, Kairi CA, Spella M, Giannou AD, Magkouta S, Giopanou I, et al. Beneficial impact of CCL2 and CCL12 neutralization on experimental malignant pleural effusion. PLoS One 2013;8:e71207.

33. Qian BZ, Li J, Zhang H, Kitamura T, Zhang J, Campion LR, et al. CCL2 recruits inflammatory monocytes to facilitate breast-tumour metastasis. Nature 2011;475:222-5.

34. Fridlender ZG, Buchlis G, Kapoor V, Cheng G, Sun J, Singhal S, et al. CCL2 blockade augments cancer immunotherapy. Cancer Res 2010;70:109-18.

35. Loberg RD, Ying C, Craig M, Day LL, Sargent E, Neeley C, et al. Targeting CCL2 with systemic delivery of neutralizing antibodies induces prostate cancer tumor regression in vivo. Cancer Res 2007;67:9417-24.

36. Brana I, Calles A, LoRusso PM, Yee LK, Puchalski TA, Seetharam S, et al. Carlumab, an anti-C-C chemokine ligand 2 monoclonal antibody, in combination with four chemotherapy regimens for the treatment of patients with solid tumors: an open-label, multicenter phase 1b study. Target Oncol 2015;10:111-23.

37. Sandhu SK, Papadopoulos K, Fong PC, Patnaik A, Messiou C, Olmos D, et al. A first-in-human, first-in-class, phase I study of carlumab (CNTO 888), a human monoclonal antibody against CC-chemokine ligand 2 in patients with solid tumors. Cancer Chemother Pharmacol 2013;71:1041-50.

38. Pienta KJ, Machiels JP, Schrijvers D, Alekseev B, Shkolnik M, Crabb SJ, et al. Phase 2 study of carlumab (CNTO 888), a human monoclonal antibody against CC-chemokine

bioRxiv preprint doi: https://doi.org/10.1101/629139; this version posted May 7, 2019. The copyright holder for this preprint (which was not certified by peer review) is the author/funder, who has granted bioRxiv a license to display the preprint in perpetuity. It is made available under aCC-BY-NC 4.0 International license.

ligand 2 (CCL2), in metastatic castration-resistant prostate cancer. Invest New Drugs 2013;31:760-8.

39. Ridker PM, Everett BM, Thuren T, MacFadyen JG, Chang WH, Ballantyne C, et al; CANTOS Trial Group. Antiinflammatory Therapy with Canakinumab for Atherosclerotic Disease. N Engl J Med 2017;377:1119-1131.

40. Ridker PM, MacFadyen JG, Thuren T, Everett BM, Libby P, Glynn RJ. Effect of interleukin–1β inhibition with canakinumab on incident lung cancer in patients with atherosclerosis: exploratory results from a randomised, double–blind, placebo–controlled trial. Lancet 2017;390:1833–42.

41. Song X, Voronov E, Dvorkin T, Fima E, Cagnano E, Benharroch D, et al. Differential effects of IL–1 alpha and IL–1 beta on tumorigenicity patterns and invasiveness. J Immunol 2003;171:6448–56.

42. Voronov E, Shouval DS, Krelin Y, Cagnano E, Benharroch D, Iwakura Y, et al. IL–1 is required for tumor invasiveness and angiogenesis. Proc Natl Acad Sci U S A 2003;100:2645–50.

43. Voigt C, May P, Gottschlich A, Markota A, Wenk D, Gerlach I, et al. Cancer cells induce interleukin–22 production from memory CD4+T cells via interleukin–1 to promote tumor growth. Proc Natl Acad Sci U S A 2017;114:12994–99.

44. Apte RN, Voronov E. Is interleukin–1 a good or bad 'guy' in tumor immunobiology and immunotherapy? Immunol Rev 2008;222:222–41.

45. Dinarello CA, Simon A, van der Meer, Jos W M. Treating inflammation by blocking interleukin–1 in a broad spectrum of diseases. Nat Rev Drug Discov 2012;11:633–52.

bioRxiv preprint doi: https://doi.org/10.1101/629139; this version posted May 7, 2019. The copyright holder for this preprint (which was not certified by peer review) is the author/funder, who has granted bioRxiv a license to display the preprint in perpetuity. It is made available under aCC-BY-NC 4.0 International license.

FIGURE LEGENDS

Figure 1. Pharmacologic evidence for *KRAS* mutation-independence *in vitro*.

Different mouse and human tumor cell lines with (red) and without (black) *Kras/KRAS* mutations (codon changes are given in parentheses) were assessed for cell viability by colorimetric WST-1-assay, for colony formation by crystal violet-stained colony counts, and for ERK phosphorylation by phospho (p)- and total (t)-ERK immunoblots after 72-hour treatments with three different KRAS inhibitors (n = 3/data-point).

(A) Graphical abstract showing molecular targets of preclinical KRAS inhibitors AA12, cysmethynil, and deltarasin.

(B-D) Fifty percent inhibitory concentrations (IC_{50}) of deltarasin (B), AA12 (C), and cysmethynil (D) by WST-1 assay.

(E, F) Representative images of colonies after saline or IC_{60} deltarasin treatment (E) and colony survival fraction (F) after IC_{60} deltarasin normalized to saline treatment.

(G, H) Quantification of normalized p-ERK/t-ERK signal change after IC_{60} deltarasin normalized to saline treatment (G) and representative immunoblots (H).

(B-D, F, G) Data presented as mean ± SD. Grey lines represent the mean of all cell lines tested, which was used to dichotomize cell lines into sensitive and resistant. *P*, probability by Fisher's exact test for cross-tabulation of *Kras/KRAS* mutation status to drug sensitivity/resistance.

KRAS, KRAS proto-oncogene GTPase; WT, wild-type; GAPDH, glyceraldehyde 3-phosphate dehydrogenase.

bioRxiv preprint doi: https://doi.org/10.1101/629139; this version posted May 7, 2019. The copyright holder for this preprint (which was not certified by peer review) is the author/funder, who has granted bioRxiv a license to display the preprint in perpetuity. It is made available under aCC-BY-NC 4.0 International license.

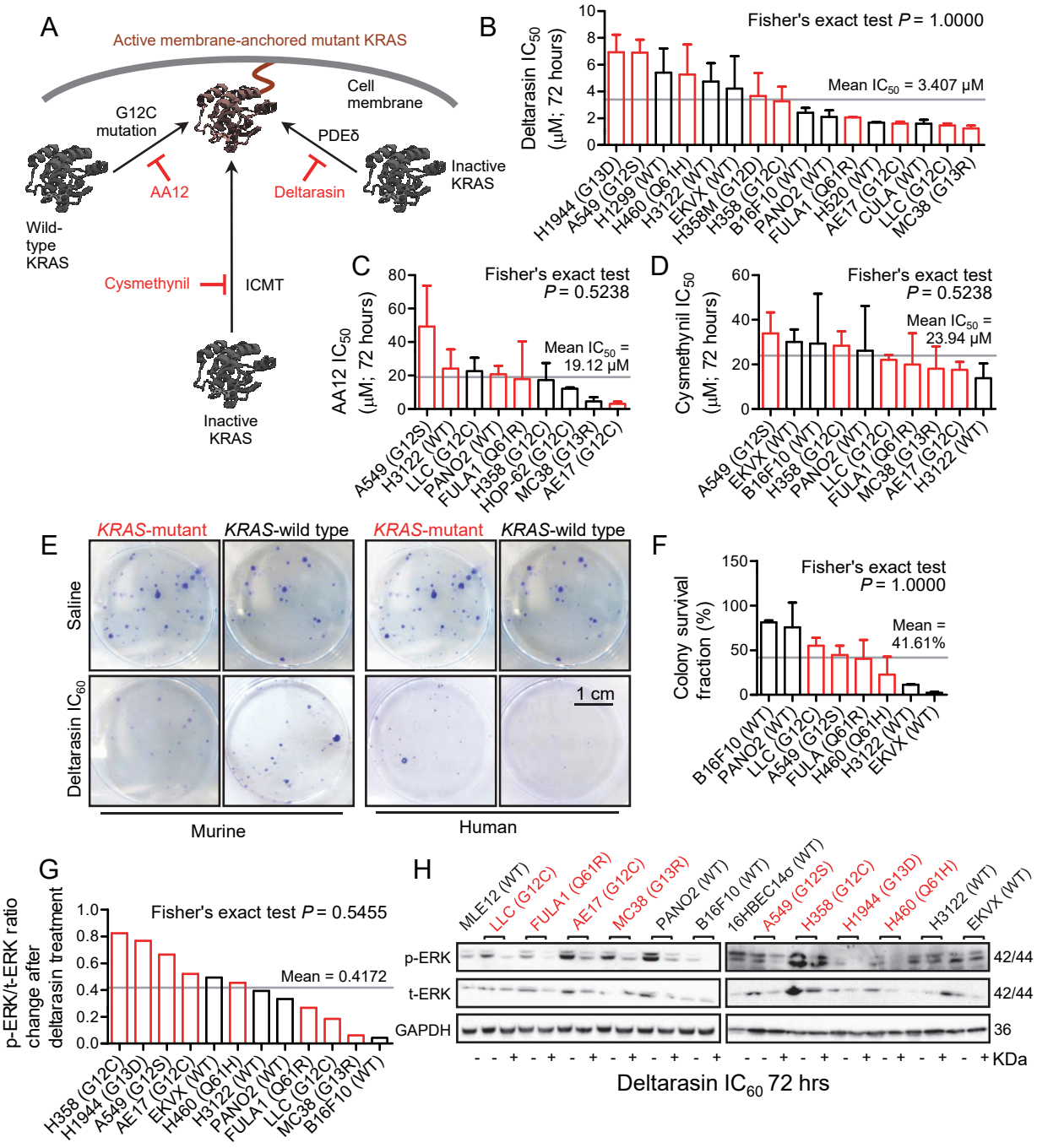

Figure 1 Arendt *et al*. In vivo-restricted effects of KRAS inhibitors.

bioRxiv preprint doi: https://doi.org/10.1101/629139; this version posted May 7, 2019. The copyright holder for this preprint (which was not certified by peer review) is the author/funder, who has granted bioRxiv a license to display the preprint in perpetuity. It is made available under aCC-BY-NC 4.0 International license.

Figure 2. Deltarasin-mediated demonstration of *KRAS* mutation-dependence *in vivo*.

Different mouse and human tumor cell lines with (**A**; $KRAS^{MUT}$) and without (**B**; $KRAS^{WT}$) endogenous *Kras/KRAS* mutations (codon changes are given in parentheses), as well as $KRAS^{WT}$ cell lines forcedly expressing a plasmid encoding mutant murine $Kras^{G12C}$ (**C**; p$Kras^{G12C}$), were injected into the rear flank (10^6 tumor cells sc) of *C57BL/6* (LLC, B16F10, and PANO2 cells), *FVB* (FULA1 cells), or *Rag2*$^{-/-}$ (H460 and EKVX cells) mice. After tumor establishment (tumor volume > 100 mm^3; arrows), mice were randomly allocated to daily ip treatments with 100 µL saline (black) or 15 mg/ Kg deltarasin in 100 µL saline (red). Tumor growth was assessed by measuring three vertical tumor dimensions.

Data presented as mean ± SD. *n*, sample size; *P*, overall probability, 2-way ANOVA; ns, **, and ***: $P > 0.05$, $P < 0.01$, and $P < 0.001$, respectively, Bonferroni post-test.

bioRxiv preprint doi: https://doi.org/10.1101/629139; this version posted May 7, 2019. The copyright holder for this preprint (which was not certified by peer review) is the author/funder, who has granted bioRxiv a license to display the preprint in perpetuity. It is made available under aCC-BY-NC 4.0 International license.

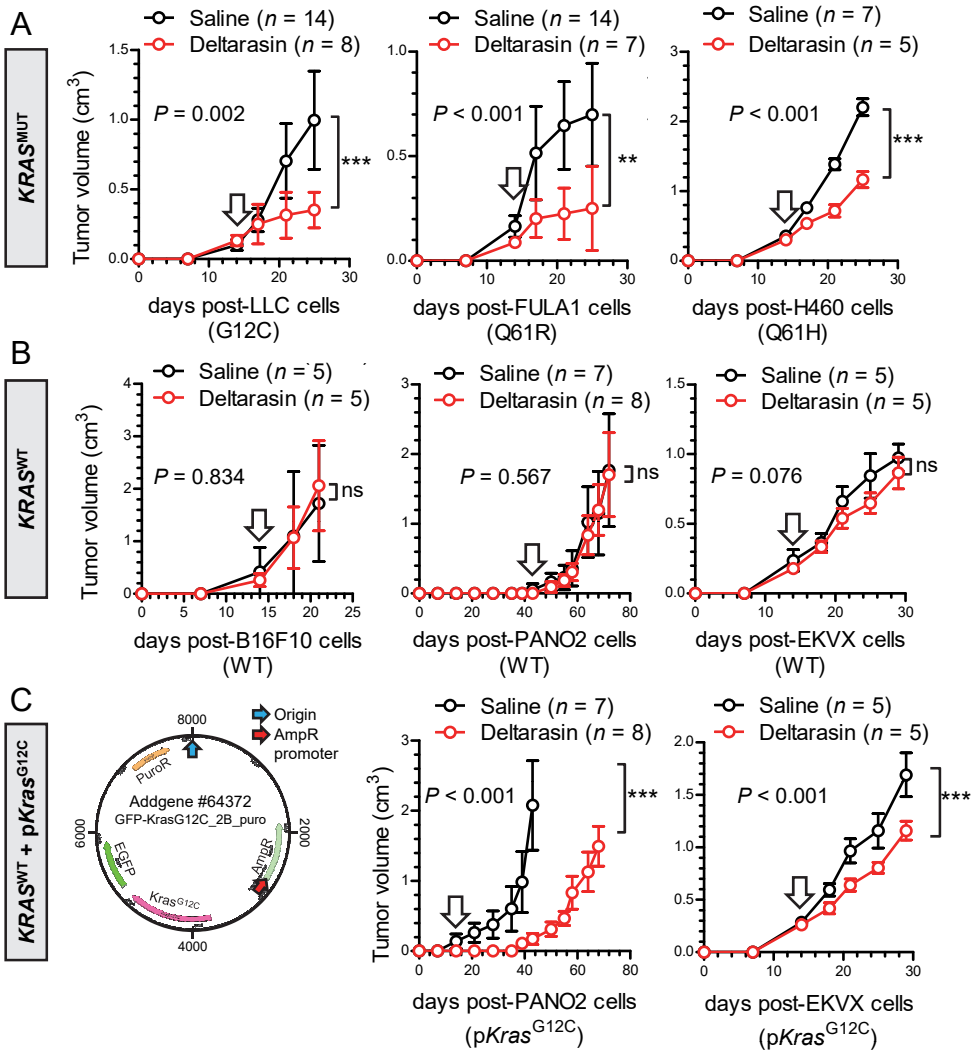

Figure 2 Arendt *et al*. In vivo-restricted effects of KRAS inhibitors.

bioRxiv preprint doi: https://doi.org/10.1101/629139; this version posted May 7, 2019. The copyright holder for this preprint (which was not certified by peer review) is the author/funder, who has granted bioRxiv a license to display the preprint in perpetuity. It is made available under aCC-BY-NC 4.0 International license.

Figure 3. Genetic manipulation of *Kras* reveals *in vivo*-restricted KRAS dependence.

(A) Different murine parental (black/grey: stably expressing random shRNA, sh*C*, or control plasmid, p*C*) or *Kras*-modified (red: stably expressing sh*Kras*; green: stably expressing mutant $Kras^{G12C}$ plasmid, p$Kras^{G12C}$) tumor cell lines were assessed for cell viability (IC_{50} by WST-1-assay; n = 2-4/data-point) after 72 hours of deltarasin treatment.

(B) Summary of averaged deltarasin IC_{50} values from all cell lines from (A) (n = 2-3 cell lines/group).

(C) Human parental (black/grey: stably expressing control plasmid p*C*) or *KRAS*-modified (green: stably expressing p$Kras^{G12C}$) tumor cell lines were assessed for cell viability by WST-1 assay (n = 2-5/data-point) after 72 hours of deltarasin treatment.

(D) Immunoblots of cell lines from (A) for p-ERK, t-ERK and GAPDH.

(E) Quantification of normalized p-ERK/t-ERK signal from (D). Dara were summarized by mutation status and origin.

(F) The five cell line doublets from (A) were injected into the rear flank (10^6 tumor cells sc) of *C57BL/6* mice for induction of flank tumors by genetically modified cells (red, sh*Kras*; green, p$Kras^{G12C}$) or control cells (black, sh*C* or p*C*).

P, overall probability by one-way (A-C) and two-way (E, F) ANOVA. ns, **, and ***: $P > 0.05$, $P < 0.01$, and $P < 0.001$, respectively, for the indicated comparisons by Bonferroni post-tests. Data are presented as mean ± SD.

bioRxiv preprint doi: https://doi.org/10.1101/629139; this version posted May 7, 2019. The copyright holder for this preprint (which was not certified by peer review) is the author/funder, who has granted bioRxiv a license to display the preprint in perpetuity. It is made available under aCC-BY-NC 4.0 International license.

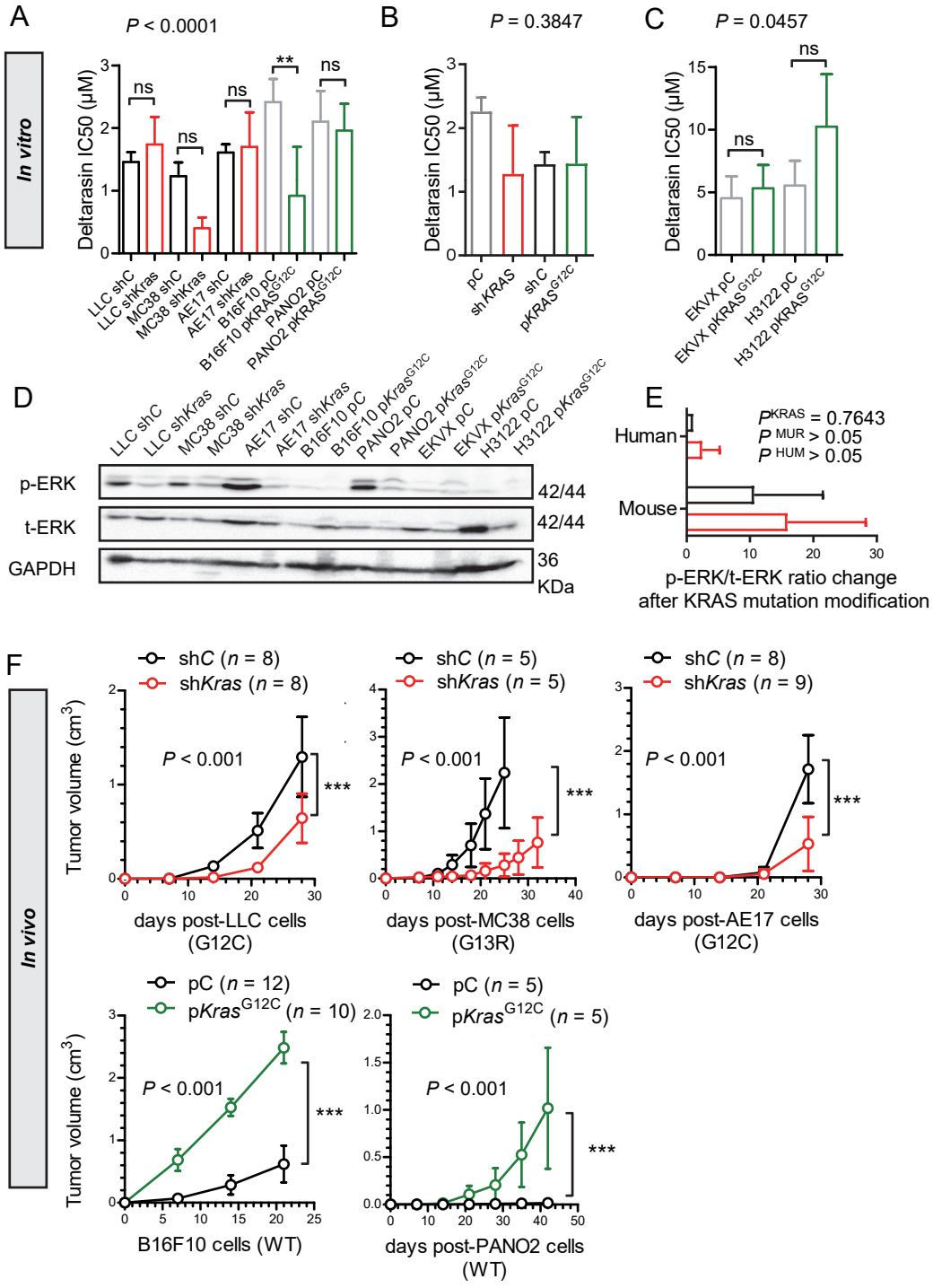

Figure 3 Arendt *et al*. In vivo-restricted effects of KRAS inhibitors.

bioRxiv preprint doi: https://doi.org/10.1101/629139; this version posted May 7, 2019. The copyright holder for this preprint (which was not certified by peer review) is the author/funder, who has granted bioRxiv a license to display the preprint in perpetuity. It is made available under aCC-BY-NC 4.0 International license.

Figure 4. A 42-gene inflammatory signature of KRAS-dependence.

(A) Unsupervised hierarchical clustering of gene expression of *Kras*-mutant and *Kras-WT* cancer cell lines, as well as benign cells and tissues.

(B) Venn diagram of analytical strategy of transcriptome analysis.

(C) Unsupervised hierarchical clustering of gene expression of *Kras*-modified cancer cell line doublets reveals co-clustering of *Il1r1* and *Ccl2*.

(D) WikiPathway analysis showing pathways significantly overrepresented in the *KRAS* signature.

(E) GSEA of 37 human orthologues of the murine *KRAS* signature against the Broad Institute's 50 hallmark signatures showing positive enrichment in the "inflammatory response" and negative enrichment in the "G2M checkpoint" signatures. NES, normalized enrichment score; *P*, family-wise error rate probability.

(F) GSEA of 37 human orthologues of the murine *KRAS* signature against KRAS- (n = 21) versus EGFR- (n = 17) -mutant lung adenocarcinomas (LADC) from BATTLE reveals positive enrichment of our KRAS signature in human *KRAS*-mutant LADC. NES, normalized enrichment score; *P*, family-wise error rate probability.

bioRxiv preprint doi: https://doi.org/10.1101/629139; this version posted May 7, 2019. The copyright holder for this preprint (which was not certified by peer review) is the author/funder, who has granted bioRxiv a license to display the preprint in perpetuity. It is made available under aCC-BY-NC 4.0 International license.

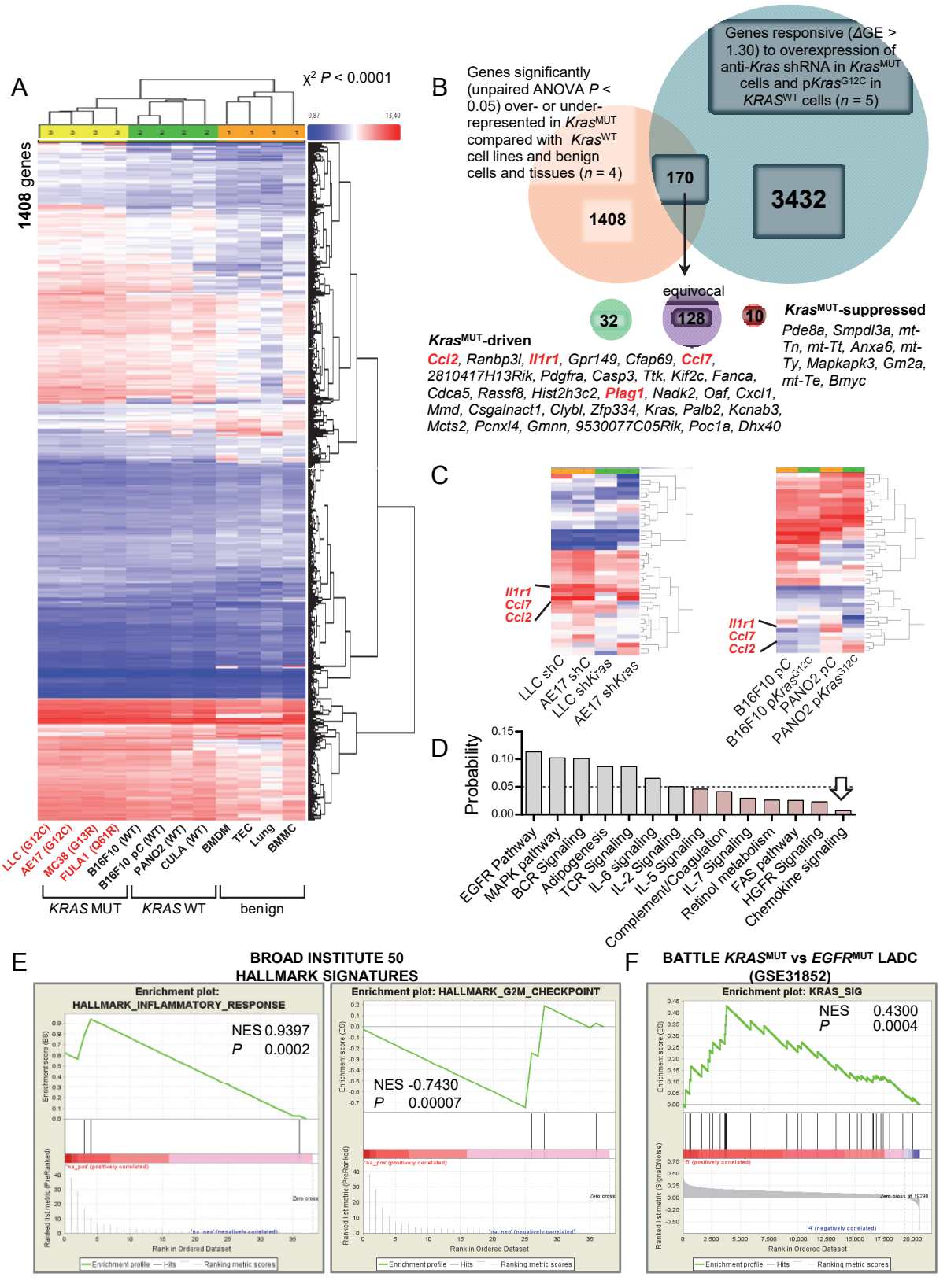

Figure 4 Arendt *et al*. In vivo-restricted effects of KRAS inhibitors.

bioRxiv preprint doi: https://doi.org/10.1101/629139; this version posted May 7, 2019. The copyright holder for this preprint (which was not certified by peer review) is the author/funder, who has granted bioRxiv a license to display the preprint in perpetuity. It is made available under aCC-BY-NC 4.0 International license.

Figure 5. A requirement for host *Ccr2* and *IL1b* for KRAS dependence *in vivo*.

(A) Graphical abstract of the proposed mechanism of *in vivo* restricted KRAS dependence.

(B) Representative image of CCR2/IL-1β-co-staining of a *KRAS*-mutant tumor from a *Rag2*$^{-/-}$ mouse showing co-localization of the two proteins in the tumor stroma. Image was taken using an AxioImager.M2 (Zeiss; Jena, Germany) and a 60x objective.

(C) Syngeneic *C57BL/6* mice competent (*WT*) or deficient (*Il1b*$^{-/-}$, *Ccr2*$^{-/-}$) [16, 18] in the *Il1b* and *Ccr2* genes or haplo/diplo-insufficient in the *Cxcr1* and *Cxcr2* chemokine receptor genes (*Cxcr1*$^{-/-}$, *Cxcr2*$^{+/-}$) received 10^6 LLC cells (*Kras*^{G12C}) sc followed by daily ip saline (black) or 15 mg/Kg deltarasin (red) treatments initiated when tumors reached 100 mm^3 volumes (arrows). Data are presented as mean ± SD. *P*, overall probabilities by 2-way ANOVA; ns, *, and ***: $P > 0.05$, $P < 0.05$, and $P < 0.001$ for the indicated comparisons by Bonferroni post-tests. Table shows animal numbers used and percentile tumor inhibition by deltarasin compared with saline.

bioRxiv preprint doi: https://doi.org/10.1101/629139; this version posted May 7, 2019. The copyright holder for this preprint (which was not certified by peer review) is the author/funder, who has granted bioRxiv a license to display the preprint in perpetuity. It is made available under aCC-BY-NC 4.0 International license.

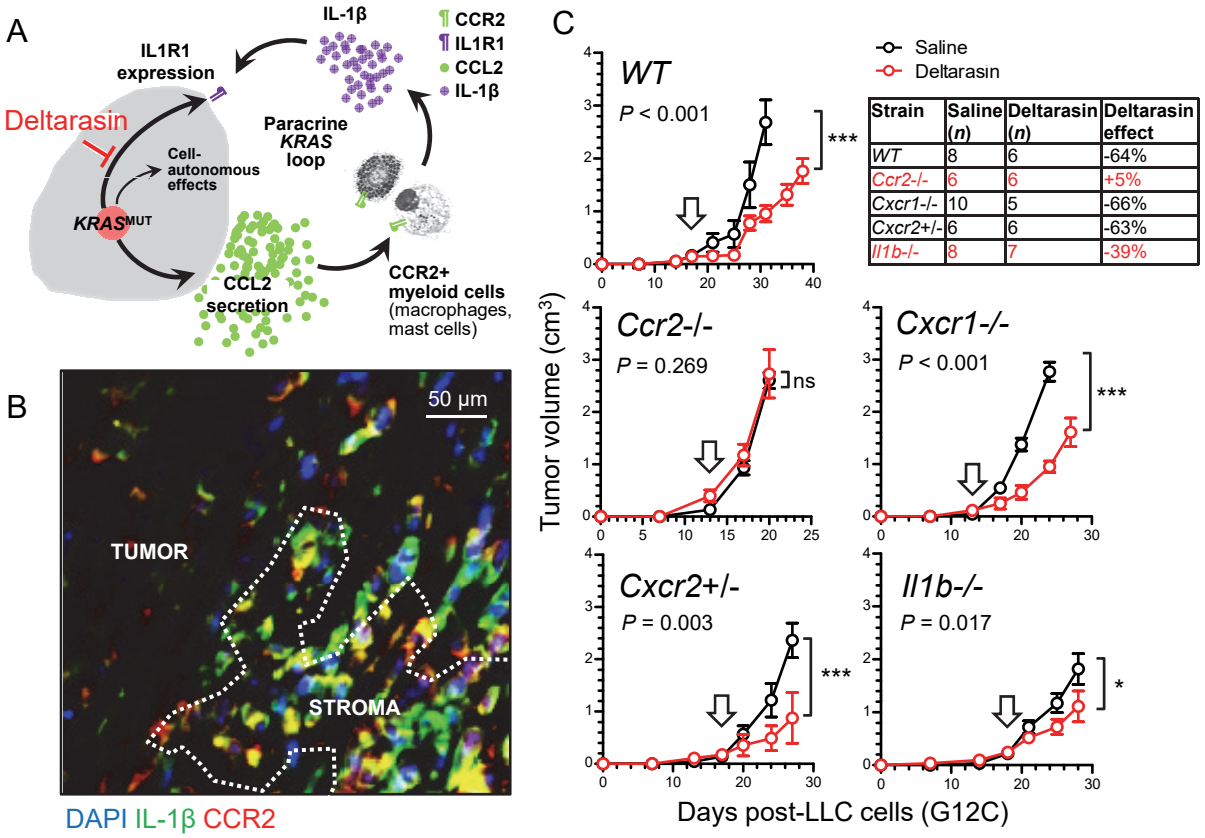

Strain	Saline (*n*)	Deltarasin (*n*)	Deltarasin effect
WT	8	6	-64%
Ccr2-/-	6	6	+5%
Cxcr1-/-	10	5	-66%
Cxcr2+/-	6	6	-63%
Il1b-/-	8	7	-39%

Figure 5 Arendt *et al*. In vivo-restricted effects of KRAS inhibitors.

bioRxiv preprint doi: https://doi.org/10.1101/629139; this version posted May 7, 2019. The copyright holder for this preprint (which was not certified by peer review) is the author/funder, who has granted bioRxiv a license to display the preprint in perpetuity. It is made available under aCC-BY-NC 4.0 International license.

Figure 6. *In vivo* KRAS-dependence requires myeloid *Ccr2* and is abolished by deltarasin treatment via downregulation of *IL1R1* expression in *KRAS*-mutant cancer cells.

(A) Total-body irradiated (900 Rad) *Ccr2*$^{-/-}$ mice received adoptive BMT from *WT* or *Ccr2*$^{-/-}$ donors (all back-crossed > F12 to the *FVB* strain). After one month allowed for chimeric bone marrow reconstitution, chimeras received 10^6 syngeneic FULA1 cells (*Kras*^{Q61R}) sc [17]. Daily ip saline or deltarasin (15 mg/Kg in saline) treatments were started when tumors > 100 mm^3 were established (arrow). Data are presented as mean ± SD. *P*, overall probabilities by 2-way ANOVA; ***: $P < 0.001$ for the indicated comparisons by Bonferroni post-tests.

(B) *Il1r1/IL1R1* mRNA expression by qPCR (top) and CCL2 protein secretion by ELISA (bottom) of mouse (left) and human (right) cancer cell lines treated with saline or deltarasin IC_{60} for 72 hours. Data are presented as mean ± SD. *P*, overall probabilities by 2-way ANOVA; ns, *, and ***: $P > 0.05$, $P < 0.05$ and $P < 0.001$, respectively, for the indicated comparisons by Bonferroni post-tests.

bioRxiv preprint doi: https://doi.org/10.1101/629139; this version posted May 7, 2019. The copyright holder for this preprint (which was not certified by peer review) is the author/funder, who has granted bioRxiv a license to display the preprint in perpetuity. It is made available under aCC-BY-NC 4.0 International license.

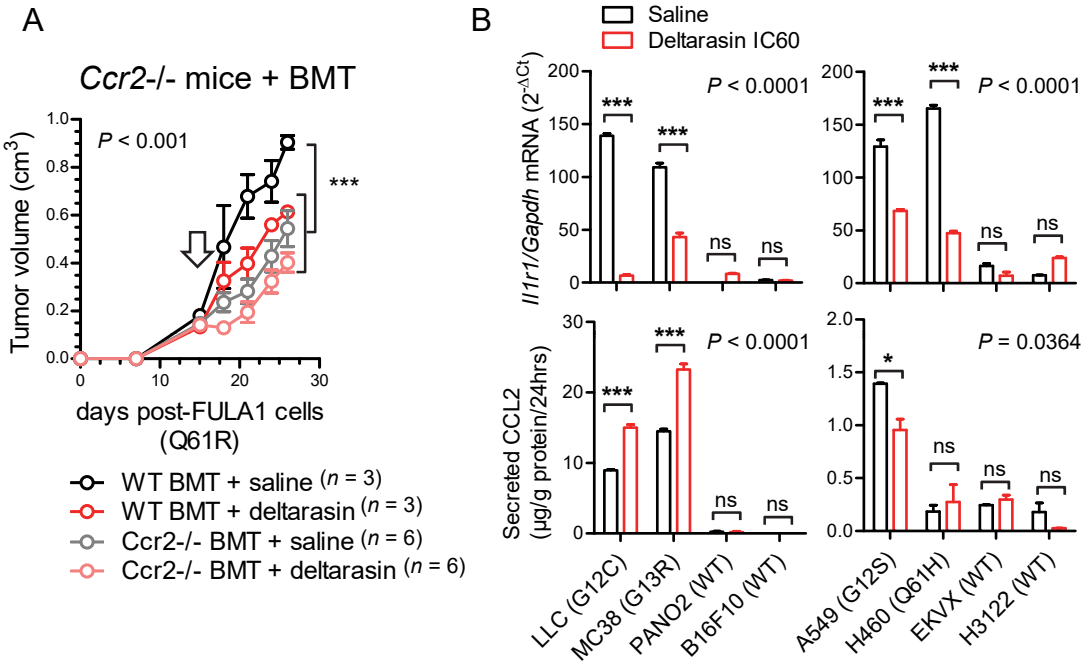

Figure 6 Arendt *et al*. In vivo-restricted effects of KRAS inhibitors.

bioRxiv preprint doi: https://doi.org/10.1101/629139; this version posted May 7, 2019. The copyright holder for this preprint (which was not certified by peer review) is the author/funder, who has granted bioRxiv a license to display the preprint in perpetuity. It is made available under aCC-BY-NC 4.0 International license.

Figure 7. Mean expression of *KRAS/CCL2/IL1B* is increased in *KRAS*-mutant cancers and predicts poor survival.

(A) Average *KRAS/CCL2/IL1B* expression normalized to *ACTB* in lung adenocarcinomas (LADC) from smokers and never-smokers and normal lung tissue from never-smokers from the BATTLE study (GSE43458) [23,24].

(B) *KRAS/CCL2/IL1B* expression normalized to *ACTB* in breast, non-small cell lung, and colorectal cancer (ROCHE study GSE103512). *KRAS* mutation frequencies of these tumor types are from COSMIC [4].

(C) Kaplan-Meier analyses of lung cancer patients stratified by average *KRAS/CCL2/IL1B* expression done on http://www.kmplot.com [19]. *KRAS* mutation frequencies are from the Campbell cohort [25]. Top: all patients; Bottom: ever-smokers only.

(A, B) Data are presented as violin plots. *P*, overall probability by one-way ANOVA. ns, *, **, and ***: $P > 0.05$, $P < 0.05$, $P < 0.01$, and $P < 0.001$, respectively, for the indicated comparisons by Bonferroni post-tests.

bioRxiv preprint doi: https://doi.org/10.1101/629139; this version posted May 7, 2019. The copyright holder for this preprint (which was not certified by peer review) is the author/funder, who has granted bioRxiv a license to display the preprint in perpetuity. It is made available under aCC-BY-NC 4.0 International license.

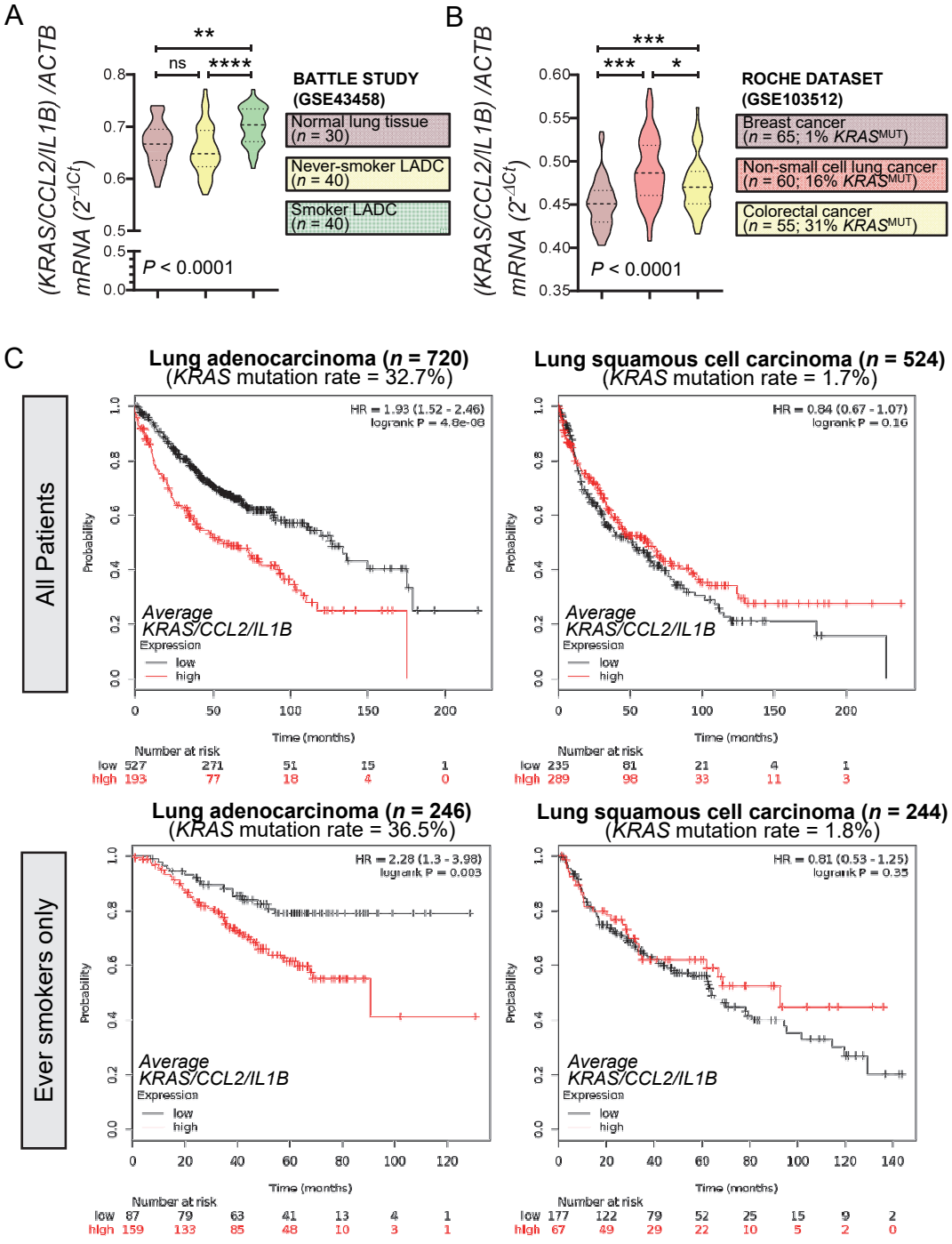

Figure 7 Arendt *et al*. In vivo-restricted effects of KRAS inhibitors.

bioRxiv preprint doi: https://doi.org/10.1101/629139; this version posted May 7, 2019. The copyright holder for this preprint (which was not certified by peer review) is the author/funder, who has granted bioRxiv a license to display the preprint in perpetuity. It is made available under aCC-BY-NC 4.0 International license.

SUPPLEMENTARY INFORMATION

An *in vivo* inflammatory loop potentiates KRAS blockade

Kristina A.M. Arendt, Giannoula Ntaliarda, Vasileios Armenis, Danai Kati, Christin Henning, Georgia A. Giotopoulou, Mario A.A. Pepe, Laura V. Klotz, Anne-Sophie Lamort, Rudolf A. Hatz, Sebastian Kobold, and Georgios T. Stathopoulos.

bioRxiv preprint doi: https://doi.org/10.1101/629139; this version posted May 7, 2019. The copyright holder for this preprint (which was not certified by peer review) is the author/funder, who has granted bioRxiv a license to display the preprint in perpetuity. It is made available under aCC-BY-NC 4.0 International license.

SUPPLEMENTARY FIGURES

Figure S1. Mutation status of cell lines used in this study, *in vitro* assays used in cancer research and comparative efficacy of KRAS versus tyrosine kinase inhibitors.

(A) Murine cell lines used in this study with their syngeneic mouse strain, tissue of origin, and mutation status of *Kras, Nras*, and *Trp53*. Data from [S1-S6].

(B) Human cell lines used in this study with their tissue of origin and mutation status of *KRAS*, *NRAS*, *ROS1*, *MAP2K1*, *TP53*, *STK11*, *NF1*, and *ARID1A*. Data from [S7].

(C) Summary of *in vitro* assays used in cancer research stratified by target gene. Data are from a PubMed search done between 17-29.07.2018 usingsearch strategy ("assay type" AND "gene" AND "cancer") and the number of retrieved publications as the readout. Assay types are listed in the x-axis and genes in the legend.MTT,3-(4,5-dimethylthiazol-2-yl)-2,5-diphenyltetrazolium bromide;MTS,3-(4,5-dimethylthiazol-2-yl)-5-(3-carboxymethoxyphenyl)-2-(4-sulfophenyl)-2H-tetrazolium); ATP, adenosine triphosphate; LDH, Lactate dehydrogenase; BrdU, bromodeoxyuridine, 5-bromo-2'-deoxyuridine**.***P*, overall probability by 2-way ANOVA. Note that MTT/MTS and colony formation assays are the most commonly used and were also used in this study.

(D) Fifty percent inhibitory concentrations (IC_{50}) of selected FDA-approved tyrosine kinase inhibitors (TKI; top) and of published KRAS inhibitors(bottom) in preclinical development. *n*, published studies; *P*, overall probability by 2-way ANOVA. Note the statistically significantly higher and physiologically difficult to achieveIC_{50} of KRAS inhibitors compared with TKI. Data were from [S8-S25].

bioRxiv preprint doi: https://doi.org/10.1101/629139; this version posted May 7, 2019. The copyright holder for this preprint (which was not certified by peer review) is the author/funder, who has granted bioRxiv a license to display the preprint in perpetuity. It is made available under aCC-BY-NC 4.0 International license.

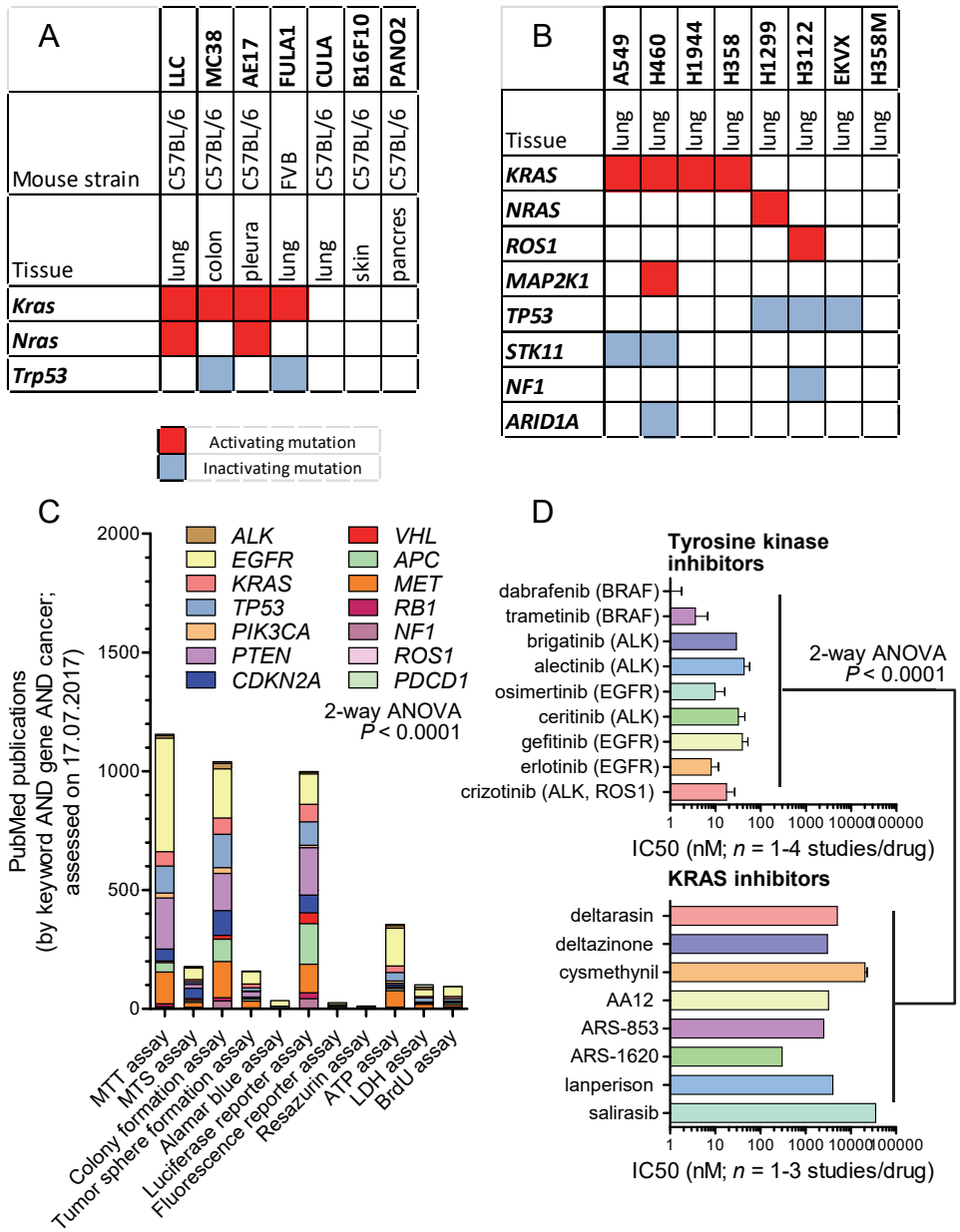

Supplementary Figure S1 Arendt *et al*. In vivo-restricted effects of KRAS inhibitors.

bioRxiv preprint doi: https://doi.org/10.1101/629139; this version posted May 7, 2019. The copyright holder for this preprint (which was not certified by peer review) is the author/funder, who has granted bioRxiv a license to display the preprint in perpetuity. It is made available under aCC-BY-NC 4.0 International license.

Figure S2. Response of *KRAS*-mutant tumor cells to *KRAS* inhibitors analyzed by WST-1 assay.

Different mouse (**A**; *Kras*^{MUT}: LLC, MC38, AE17, FULA1; *Kras*^{WT}: B16F10, CULA, PANO2) and human (**B**; *KRAS*^{MUT}: A549, H460, H358, H358M, H1944, HOP-62; *KRAS*^{WT}: EKVX, H1299, H3122, H520) tumor cell lines were assessed for inhibition of cell viability (determined by WST-1 assay, n = 3/data-point) by three different KRAS inhibitors: deltarasin (top), AA12 (middle), and cysmethynil (bottom).

Data presented as mean ± SD. *P*, overall probability by nonlinear fit and extra sum of squares F-test.

bioRxiv preprint doi: https://doi.org/10.1101/629139; this version posted May 7, 2019. The copyright holder for this preprint (which was not certified by peer review) is the author/funder, who has granted bioRxiv a license to display the preprint in perpetuity. It is made available under aCC-BY-NC 4.0 International license.

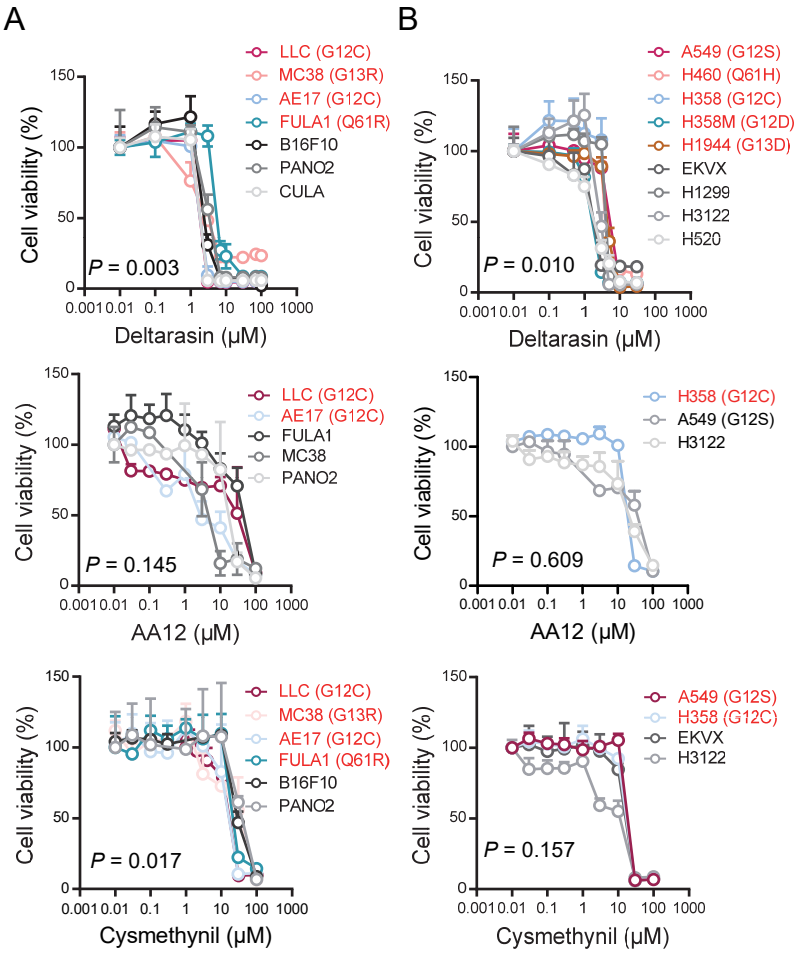

Supplementary Figure S2 Arendt *et al*. In vivo-restricted effects of KRAS inhibitors.

bioRxiv preprint doi: https://doi.org/10.1101/629139; this version posted May 7, 2019. The copyright holder for this preprint (which was not certified by peer review) is the author/funder, who has granted bioRxiv a license to display the preprint in perpetuity. It is made available under aCC-BY-NC 4.0 International license.

Figure S3. Response of *KRAS*-mutant tumor cells to *KRAS* inhibitors analyzed by colony formation assay.

Different mouse (**A**; $Kras^{MUT}$: LLC, FULA1; $Kras^{WT}$: B16F10, PANO2) and human (**B**; $KRAS^{MUT}$: A549, H460; $KRAS^{WT}$: EKVX, H3122) tumor cell lines were assessed for colony formation (n = 3/ data-point) after 72 h of saline or deltarasin treatment.

Data presented as mean ± SD. P, overall probability by one-way ANOVA. * and ***: $P< 0.05$ and $P< 0.001$, respectively, for the indicated comparisons by Bonferroni post-tests. Shown are total number of colonies formed(top), plating efficiency of 300 cells/well at experiment start (middle), and survival fraction of single cells given as ratio treatment/no treatment.

bioRxiv preprint doi: https://doi.org/10.1101/629139; this version posted May 7, 2019. The copyright holder for this preprint (which was not certified by peer review) is the author/funder, who has granted bioRxiv a license to display the preprint in perpetuity. It is made available under aCC-BY-NC 4.0 International license.

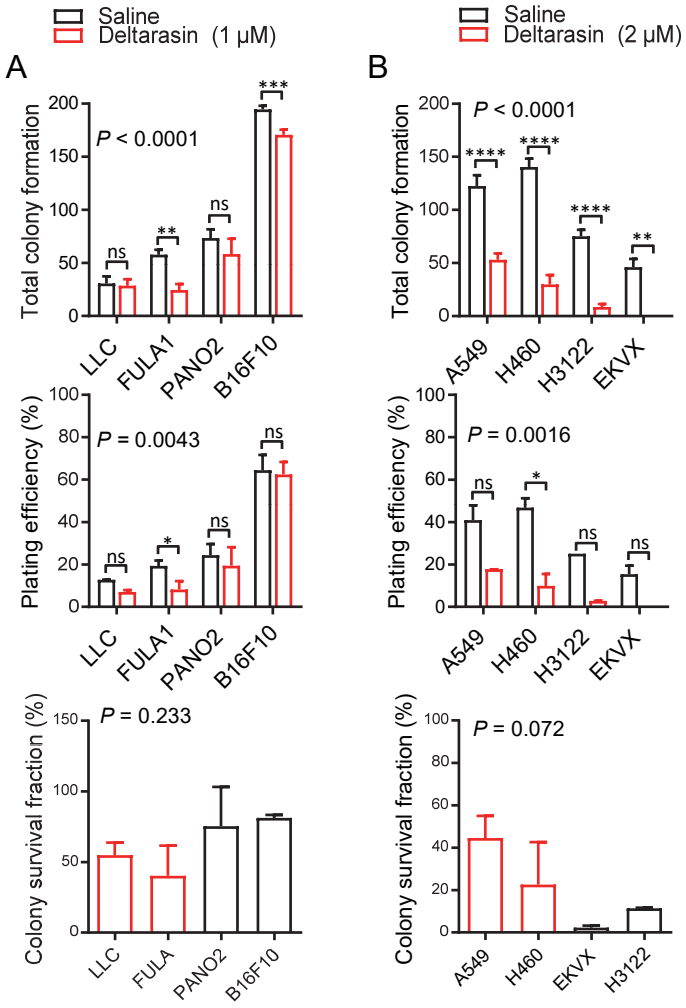

Supplementary Figure S3 Arendt *et al*. In vivo-restricted effects of KRAS inhibitors.

bioRxiv preprint doi: https://doi.org/10.1101/629139; this version posted May 7, 2019. The copyright holder for this preprint (which was not certified by peer review) is the author/funder, who has granted bioRxiv a license to display the preprint in perpetuity. It is made available under aCC-BY-NC 4.0 International license.

Figure S4. Uncropped blots for Figure 1H.

(A) Immunoblots of murine cell line protein extracts untreated and treated with deltarasin (72 h; IC_{60}). Left, p-ERK, t-ERK; right, GAPDH.

(B) Immunoblots of human cell line protein extracts untreated and treated with deltarasin (72 h; IC_{60}). Left, p-ERK, t-ERK; right, GAPDH.
Dashed lines represent areas of the blots shown in main Figure.

bioRxiv preprint doi: https://doi.org/10.1101/629139; this version posted May 7, 2019. The copyright holder for this preprint (which was not certified by peer review) is the author/funder, who has granted bioRxiv a license to display the preprint in perpetuity. It is made available under aCC-BY-NC 4.0 International license.

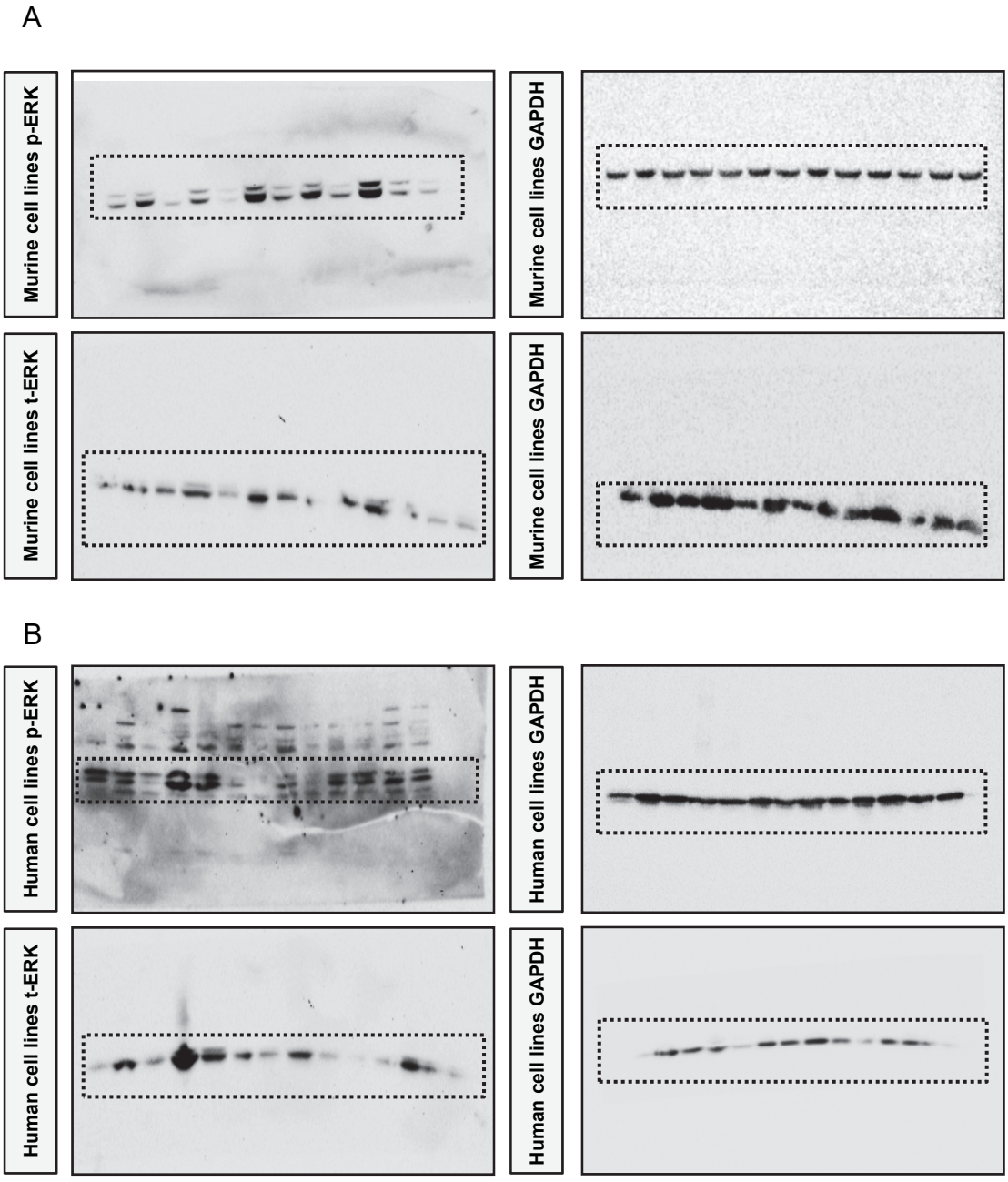

Supplementary Figure S4 Arendt *et al*. In vivo-restricted effects of KRAS inhibitors.

bioRxiv preprint doi: https://doi.org/10.1101/629139; this version posted May 7, 2019. The copyright holder for this preprint (which was not certified by peer review) is the author/funder, who has granted bioRxiv a license to display the preprint in perpetuity. It is made available under aCC-BY-NC 4.0 International license.

Figure S5. Validation of p*Kras*^{G12C} transduction in human cell lines H3122 and EKVX.

The p*Kras*^{G12C} plasmid includes GFP and puromycin resistance genes. Representative microscopy images of p*C* control or p*Kras*^{G12C} transfected cell lines. Left, brightfield images; middle, green fluorescent images; right, merged images. Images were taken with a confocal microscope LCI510 (Zeiss; Jena, Germany).

bioRxiv preprint doi: https://doi.org/10.1101/629139; this version posted May 7, 2019. The copyright holder for this preprint (which was not certified by peer review) is the author/funder, who has granted bioRxiv a license to display the preprint in perpetuity. It is made available under aCC-BY-NC 4.0 International license.

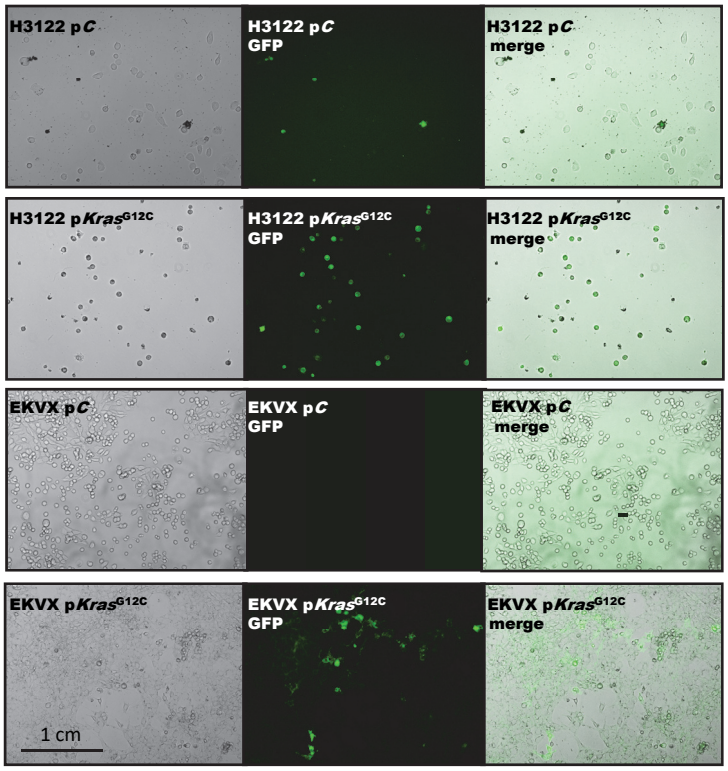

Supplementary Figure S5 Arendt *et al*. In vivo-restricted effects of KRAS inhibitors.

bioRxiv preprint doi: https://doi.org/10.1101/629139; this version posted May 7, 2019. The copyright holder for this preprint (which was not certified by peer review) is the author/funder, who has granted bioRxiv a license to display the preprint in perpetuity. It is made available under aCC-BY-NC 4.0 International license.

Figure S6. Uncropped blots for Figure 3D.

Immunoblots of murine and human cell line protein extracts with or without *Kras/KRAS* genetic modification. Left, p-ERK, t-ERK; right, GAPDH. Dashed lines represent areas of the blots shown in main Figure.

bioRxiv preprint doi: https://doi.org/10.1101/629139; this version posted May 7, 2019. The copyright holder for this preprint (which was not certified by peer review) is the author/funder, who has granted bioRxiv a license to display the preprint in perpetuity. It is made available under aCC-BY-NC 4.0 International license.

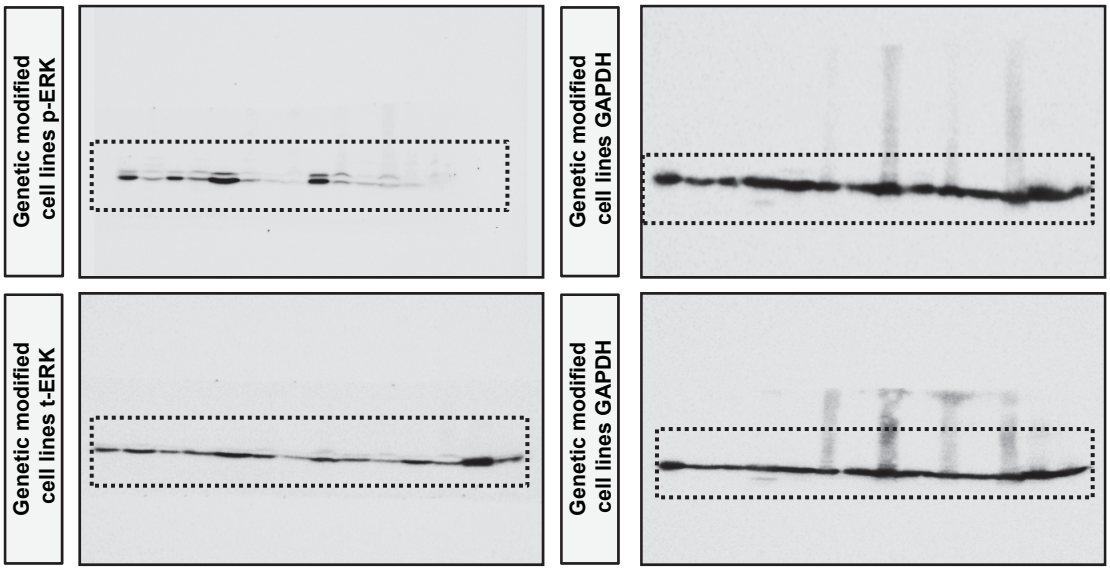

Supplementary Figure S6 Arendt *et al*. In vivo-restricted effects of KRAS inhibitors.

bioRxiv preprint doi: https://doi.org/10.1101/629139; this version posted May 7, 2019. The copyright holder for this preprint (which was not certified by peer review) is the author/funder, who has granted bioRxiv a license to display the preprint in perpetuity. It is made available under aCC-BY-NC 4.0 International license.

SUPPLEMENTARY TABLES

Supplementary Table S1. Antibodies used in this study.

Method[a]	Target protein	Provider	Catalog number	Dilution
WB	p-ERK	Santa Cruz Biotechnology	sc-7383	1:1000
WB	t-ERK	Santa Cruz Biotechnology	sc-514302	1:1000
WB	GAPDH	Cell Signaling	#2118	1:2000
WB	rat anti-mouse IgG	Abcam	ab131368	1:10000
WB	anti-rabbit IgG VHH	Abcam	ab191866	1:10000
IF	IL-1ß-Alexa488	Santa Cruz Biotechnology	sc-5155988 AF488	1:50
IF	CCR2	Thermo Fisher Scientific	PA5-23043	1:50
IF	donkey anti-rabbit IgG AlexaFluor647	Abcam	ab150075	1:500
IF	normal mouse IgG2a Alexa Fluor488	Santa Cruz Biotechnology	sc-3891	1:50
IF	normal mouse IgG1 Alexa Fluor488	Santa Cruz Biotechnology	sc-3890	1:50

bioRxiv preprint doi: https://doi.org/10.1101/629139; this version posted May 7, 2019. The copyright holder for this preprint (which was not certified by peer review) is the author/funder, who has granted bioRxiv a license to display the preprint in perpetuity. It is made available under aCC-BY-NC 4.0 International license.

Supplementary Table S2. Oligonucleotides for qPCR.

Primer	**Sequence**	**Amplicon (bp)**
Murine *Il1r1*F	GCTGACTTGAGGCAGTT	200
Murine *Il1r1*R	CATACGTCAATCTCCAGCGAC	
Human *IL1R1*F	AGGTAGACGCACCCTCTGAA	154
Human *IL1R1*R	GCATTTATCAGCCTCCAGAGAAG	
Murine *Gapdh*F	CCCTTAAGAGGGATGCTGCC	124
Murine *Gapdh*R	TACGGCCAAATCCGTTCACA	
Human *GAPDH*F	TTAGGAAAGCCTGCCGGTGA	157
Human *GAPDH*R	GGCGCCCAATACGACCAAA	

bioRxiv preprint doi: https://doi.org/10.1101/629139; this version posted May 7, 2019. The copyright holder for this preprint (which was not certified by peer review) is the author/funder, who has granted bioRxiv a license to display the preprint in perpetuity. It is made available under aCC-BY-NC 4.0 International license.

SupplementaryTable S3.Deltarasin effects on a battery of murine and human cancer cell lines.

Originating oganism	**Cell line**	**Tissue origin**	***KRAS* mutation**	**IC_{50} (µM, mean±SD)[a]**	***n***
C57BL/6 mouse	LLC	Lewis lung carcinoma	G12C	1.46 ± 0.16	3
C57BL/6 mouse	MC38	Colon adenocarcinoma	G13R	1.23 ± 0.22	3
C57BL/6 mouse	AE17	Malignat pleural mesothelioma	G12C	1.61 ± 0.13	3
FVB mouse	FULA	Urethane-induced lung adenocarcinoma	Q61R	2.10 ± 0.06	3
C57BL/6 mouse	B16F10	Malignant skin melanoma	None	2.41 ± 0.37	3
C57BL/6 mouse	PANO2	Pancreatic adenocarcinoma	None	2.10 ± 0.49	4
C57BL/6 mouse	CULA	Urethane-induced lung adenocarcinoma	None	1.59 ± 0.29	3
Human	A549	Lung adenocarcinoma	G12S	6.90 ± 0.96	3
Human	H460	Lung large cell carcinoma	Q61H	5.27 ± 2.24	3
Human	H358	NSCLC	G12C	3.27 ±1.10	3
Human	H358M	Bronchiolo-alveolar carcinoma	G12D	3.67 ± 1.70	3
Human	H1944	NSCLC	G13D	6.93 ± 1.32	3
Human	H520	Squamous cell carcinoma	None	1.67 ± 0.06	3
Human	EKVX	Lung adenocarcinoma	None	4.22 ± 2.41	3
Human	H1299	NSCLC	None	5.40 ± 1.81	3
Human	H3122	NSCLC	None	4.73 ± 1.38	3

[a] IC_{50}, 50% inhibitory concentration by WST-1 assay (Biotool); SD, standard deviation; *n*, sample size; NSCLC, non-small cell lung cancer.

bioRxiv preprint doi: https://doi.org/10.1101/629139; this version posted May 7, 2019. The copyright holder for this preprint (which was not certified by peer review) is the author/funder, who has granted bioRxiv a license to display the preprint in perpetuity. It is made available under aCC-BY-NC 4.0 International license.

Supplementary Table S4. AA12 effects on a battery of murine and human cancer cell lines.

Originating oganism	**Cell line**	**Tissue origin**	***KRAS* mutation**	**IC_{50} (μM, mean±SD)[a]**	***n***
C57BL/6 mouse	LLC	Lewis lung carcinoma	G12C	22.69 ± 7.95	3
C57BL/6 mouse	MC38	Colon adenocarcinoma	G13R	4.59 ± 2.45	2
C57BL/6 mouse	AE17	Malignant pleural mesothelioma	G12C	3.06 ± 1.39	2
FVB mouse	FULA1	Urethane-induced lung adenocarcinoma	Q61R	4.97 ± 2.28	2
C57BL/6 mouse	PANO2	Pancreatic adenocarcinoma	None	20.85 ± 5.11	2
Human	A549	Lung adenocarcinoma	G12S	49.30 ± 24.31	3
Human	H358	NSCLC	G12C	27.85 ± 4.41	2
Human	H3122	NSCLC	None	24.24 ± 11.41	3

[a] IC_{50}, 50% inhibitory concentration by WST-1 assay (Biotool); SD, standard deviation; *n*, sample size; NSCLC, non-small cell lung cancer.

bioRxiv preprint doi: https://doi.org/10.1101/629139; this version posted May 7, 2019. The copyright holder for this preprint (which was not certified by peer review) is the author/funder, who has granted bioRxiv a license to display the preprint in perpetuity. It is made available under aCC-BY-NC 4.0 International license.

Supplementary Table S5. Cysmethynil effects on a battery of murine and human cancer cell lines.

Originating oganism	**Cellline**	**Tissue origin**	***KRAS* mutation**	**IC_{50} (µM, mean±SD)[a]**	***n***
C57BL/6 mouse	LLC	Lewis lung carcinoma	G12C	22.11 ± 2.19	2
C57BL/6 mouse	MC38	Colon adenocarcinoma	G13R	18.13 ± 9.92	2
C57BL/6 mouse	AE17	Malignant pleural mesothelioma	G12C	17.62 ± 3.57	3
FVB mouse	FULA1	Urethane-induced lung adenocarcinoma	Q61R	27.37 ± 7.78	2
C57BL/6 mouse	B16F10	Malignant skin melanoma	None	19.61 ± 13.27	3
C57BL/6 mouse	PANO2	Pancreatic adenocarcinoma	None	16.92 ± 17.22	2
Human	A549	Lung adenocarcinoma	G12S	30.84 ± 9.10	3
Human	H358	NSCLC	G12C	28.32 ± 6.57	3
Human	EKVX	Lung adenocarcinoma	None	30.05 ± 5.66	3
Human	H3122	NSCLC	None	10.95 ± 3.77	3

[a] IC_{50}, 50% inhibitory concentration by WST-1 assay (Biotool); SD, standard deviation; *n*, sample size; NSCLC, non-small cell lung cancer.

bioRxiv preprint doi: https://doi.org/10.1101/629139; this version posted May 7, 2019. The copyright holder for this preprint (which was not certified by peer review) is the author/funder, who has granted bioRxiv a license to display the preprint in perpetuity. It is made available under aCC-BY-NC 4.0 International license.

Supplementary Table S6. A 42-gene mutant *KRAS* signature identified from microarray analyses.

Genes significantly ($P < 0.05$ by unpaired ANOVA with Bonferroni post-tests) differentially represented in *KRAS*-mutant tumor cells compared with *KRAS*-wild-type tumor cells and benign cells and tissues, at the same time >30% responsive to modulation of *KRAS* expression in all five tumor cell line doublets tested (LLC, MC38, and AE17 cells expressing sh*C* versus sh*Kras* and PANO2 and B16F10 cells expressing p*C* versus p*Kras*^{G12C}).

Gene Symbol	Description	*Kras*^{WTa}	*Kras*^{MUTb}	% *Kras*^{Rc}
Ccl2	chemokine (C-C motif) ligand 2	0.82	37.79	56.29
Ranbp3l	RAN binding protein 3-like	0.93	35.26	78.33
Il1r1	interleukin 1 receptor, type I	2.39	25.63	36.71
Gpr149	G protein-coupled receptor 149	0.80	22.94	55.68
Cfap69	cilia and flagella associated protein 69	4.50	20.11	40.29
Ccl7	chemokine (C-C motif) ligand 7	0.96	16.11	50.14
2810417H13Rik	RIKEN cDNA 2810417H13 gene	11.39	12.64	42.33
Pdgfra	platelet derived growth factor receptor α	1.89	12.38	41.60
Casp3	caspase 3	4.20	10.48	30.74
Ttk	Ttk protein kinase	7.94	9.58	45.13
Kif2c	kinesin family member 2C	5.98	7.78	45.06
Fanca	Fanconi anemia, complementation group A	4.00	5.58	46.78
Cdca5	cell division cycle associated 5	3.56	5.43	47.15
Rassf8	Ras association (RalGDS/AF-6) domain family (N-terminal) member 8	2.46	5.35	32.08
Hist2h3c2	histone cluster 2, H3c2	1.20	4.69	38.87
Plag1	pleiomorphic adenoma gene 1	0.78	4.53	53.15
Nadk2	NAD kinase 2, mitochondrial	1.58	4.50	50.89
Oaf	OAF homolog (Drosophila)	2.39	4.23	31.03
Cxcl1	chemokine (C-X-C motif) ligand 1	1.56	4.23	73.09
Mmd	monocyte to macrophage differentiation-associated	2.93	4.06	35.92
Csgalnact1	chondroitin sulfate N-acetylgalactosaminyltransferase 1	0.74	3.97	50.96
Clybl	citrate lyase beta like	1.72	3.76	42.33
Zfp334	zinc finger protein 334	1.04	3.68	58.59
Kras	v-Ki-ras2 Kirsten rat sarcoma viral oncogene homolog	2.08	2.60	39.71
Palb2	partner and localizer of BRCA2	2.39	2.57	30.55
Kcnab3	potassium voltage-gated channel, shaker-related subfamily, beta member 3	1.25	2.55	49.23
Mcts2	malignant T cell amplified sequence 2	1.45	2.36	30.65
Pcnxl4	pecanex-like 4 (Drosophila)	1.38	2.19	39.54
Gmnn	geminin	1.39	2.04	34.57

bioRxiv preprint doi: https://doi.org/10.1101/629139; this version posted May 7, 2019. The copyright holder for this preprint (which was not certified by peer review) is the author/funder, who has granted bioRxiv a license to display the preprint in perpetuity. It is made available under aCC-BY-NC 4.0 International license.

9530077C05Rik	RIKEN cDNA 9530077C05 gene	1.17	1.88	30.46
Poc1a	POC1 centriolar protein homolog A	1.46	1.68	36.71
Dhx40	DEAH (Asp-Glu-Ala-His) box polypeptide 40	1.28	1.67	31.03
Pde8a	phosphodiesterase 8A	1.54	0.23	-181.67
mt-Tt	mitochondriallyencoded tRNA theonine	0.78	0.22	-95.34
Mapkapk3	mitogen-activated protein kinase-activated protein kinase 3	0.60	0.20	-96.43
Anxa6	annexin A6	0.69	0.19	-76.05
mt-Te	mitochondrially encoded tRNA glutamic acid	0.33	0.16	-49.69
mt-Ty	mitochondriallyencoded tRNA tyrosine	0.22	0.15	-77.77
Bmyc	brain expressed myelocytomatosis oncogene	1.42	0.15	-71.71
Gm2a	GM2 ganglioside activator protein	0.40	0.12	-70.05
Smpdl3a	sphingomyelin phosphodiesterase, acid-like 3A	1.21	0.11	-123.77
mt-Tn	mitochondriallyencoded tRNA asparagine	0.33	0.11	-105.91

[a] Normalized mRNA expression levels of *Kras*-wild-type (WT) cell lines (B16F10, B16F10 stably expressing p*C*, PANO2, and CULA cells) shown as fraction of expression of benign cells (bone marrow-derived macrophages and mast cells, tracheal epithelial cells) and lungs (n = 4/group).

[b] Normalized mRNA expression levels of *Kras*-mutant (MUT) cell lines (LLC, MC38, AE17, and FULA cells) shown as fraction of expression of benign cells (bone marrow-derived macrophages and mast cells, tracheal epithelial cells) and lungs (n = 4/group).

[c] Percentile mean response (R) of mRNA expression levels to *Kras* modulation, including *Kras* silencing of *Kras*-mutant cell lines (LLC, MC38, and AE17 cells) and overexpression of mutant $Kras^{G12C}$ plasmid in *Kras*-wild-type cells (B16F10 and PANO2 cells). Positive responses indicate suppression by *Kras* silencing and induction by overexpression of mutant $Kras^{G12C}$ plasmid. Negative responses indicate induction by *Kras* silencing and suppression by overexpression of mutant $Kras^{G12C}$ plasmid.

LLC, *C57BL/6* Lewis lung carcinoma; MC38, *C57BL/6* colon adenocarcinoma; AE17, *C57BL/6* malignant pleural mesothelioma; FULA, *FVB* urethane-induced lung adenocarcinoma; B16F10, *C57BL/6* malignant skin melanoma; PANO2, *C57BL/6* pancreatic adenocarcinoma; CULA, *C57BL/6* urethane-induced lung adenocarcinoma.

bioRxiv preprint doi: https://doi.org/10.1101/629139; this version posted May 7, 2019. The copyright holder for this preprint (which was not certified by peer review) is the author/funder, who has granted bioRxiv a license to display the preprint in perpetuity. It is made available under aCC-BY-NC 4.0 International license.

SUPPLEMENTARY REFERENCES

S1. Agalioti T, Giannou AD, Krontira AC, Kanellakis NI, Kati D, Vreka M, *et al*. Mutant KRAS promotes malignant pleural effusion formation. *Nat Commun* **2017**;8:15205.

S2. Marazioti A, Lilis I, Vreka M, Apostolopoulou H, Kalogeropoulou A, Giopanou I,*et al*. Myeloid-derived IL-1ß drives oncogenic KRAS-NF-kB addiction in malignant pleural effusion. *Nat Commun* **2018**; 9:672.

S3. Giannou AD, Marazioti A, Kanellakis NI, Giopanou I, Lilis I, Zazara DE, *et al*. *NRAS* destines tumor cells to the lungs. *EMBO Mol Med***2017**;9:672–686.

S4. Giopanou I, Lilis I, Papaleonidopoulos V, Agalioti T, Kanellakis NI, Spiropoulou N, *et al*. Tumor–derived osteopontin isoforms cooperate with TRP53 and CCL2 to promote lung metastasis. *Oncoimmunology* **2017**;6:e1256528.

S5. Kanellakis NI, Giannou AD, Pepe MA, Agalioti T, Zazara DE, Giopanou I, *et al*. Tobacco chemical-induced mouse lung adenocarcinoma cell lines pin the prolactin orthologue proliferin as a lung tumour promoter. *Carcinogenesis* **2019** Mar 4. pii: bgz047. doi: 10.1093/carcin/bgz047.

S6. Giannou AD, Marazioti A, Spella M, Kanellakis NI, Apostolopoulou H, Psallidas I, *et al*. Mast cells mediate malignant pleural effusion formation. *J Clin Invest* **2015**;125:2317–34.

S7. Tate JG, Bamford S, Jubb HC, Sondka Z, Beare DM, Bindal N, *et al*. COSMIC: the Catalogue Of Somatic Mutations In Cancer. *Nucleic Acids Res* **2019**;47:D941–D947.

S8. Hong S, Hong S, Han SB. Overcoming metastatic melanoma with BRAF inhibitors. *Arch Pharm Res* **2011**;34:699-701.

S9. Yamaguchi T, Kakefuda R, Tajima N, Sowa Y, Sakai T. Antitumor activities of JTP-74057 (GSK1120212), a novel MEK1/2 inhibitor, on colorectal cancer cell lines in vitro and in vivo. *Int J Oncol* **2011**;39:23-31.

S10. Hirano T, Yasuda H, Tani T, Hamamoto J, Oashi A, Ishioka K, *et al*. In vitro modeling to determine mutation specificity of EGFR tyrosine kinase inhibitors against clinically relevant EGFR mutants in non-small-cell lung cancer. *Oncotarget***2015**;6:38789-803.

S11. Sakamoto H, Tsukaguchi T, Hiroshima S, Kodama T, Kobayashi T, Fukami TA, *et al*. CH5424802, a selective ALK inhibitor capable of blocking the resistant gatekeeper mutant. *Cancer Cell* **2011**;19:679-90.

S12. Huang WS, Liu S, Zou D, Thomas M, Wang Y, Zhou T, *et al*. Discovery of Brigatinib (AP26113), a Phosphine Oxide-Containing, Potent, Orally Active Inhibitor of Anaplastic Lymphoma Kinase. *J Med Chem* **2016**;59:4948-64.

S13. Chen J, Jiang C, Wang S. LDK378: a promising anaplastic lymphoma kinase (ALK)

bioRxiv preprint doi: https://doi.org/10.1101/629139; this version posted May 7, 2019. The copyright holder for this preprint (which was not certified by peer review) is the author/funder, who has granted bioRxiv a license to display the preprint in perpetuity. It is made available under aCC-BY-NC 4.0 International license.

inhibitor. *J Med Chem* **2013**;56:5673-4.

S14. Prahallad A, Sun C, Huang S, Di Nicolantonio F, Salazar R, Zecchin D, *et al*. Unresponsiveness of colon cancer to BRAF(V600E) inhibition through feedback activation of EGFR. *Nature* **2012**;483:100-3.

S15. Wilson TR, Fridlyand J, Yan Y, Penuel E, Burton L, Chan E, *et al*. Widespread potential for growth-factor-driven resistance to anticancer kinase inhibitors. *Nature* **2012**;487:505-9.

S16. Zhang Z, Lee JC, Lin L, Olivas V, Au V, LaFramboise T, *et al.* Activation of the AXL kinase causes resistance to EGFR–targeted therapy in lung cancer. *Nat Genet* **2012**;44:852–60.

S17. Zhang F, Cheong JK. The renewed battle against RAS-mutant cancers. *Cell Mol Life Sci* **2016**;73:1845-58.

S18. Lito P, Solomon M, Li LS, Hansen R, Rosen N. Allele-specific inhibitors inactivate mutant KRAS G12C by a trapping mechanism. *Science* **2016**;351:604-8.

S19. Ostrem JM, Peters U, Sos ML, Wells JA, Shokat KM. K-Ras(G12C) inhibitors allosterically control GTP affinity and effector interactions. *Nature* **2013**;503:548–51.

S20. Winter–Vann AM, Baron RA, Wong W, dela Cruz J, York JD, Gooden DM, *et al*. A small–molecule inhibitor of isoprenylcysteine carboxyl methyltransferase with antitumor activity in cancer cells. *Proc Natl Acad Sci U S A* **2005**;102:4336–41

S21. Wang M, Hossain MS, Tan W, Coolman B, Zhou J, Liu S, *et al.* Inhibition of isoprenylcysteine carboxylmethyltransferase induces autophagic–dependent apoptosis and impairs tumor growth. *Oncogene* **2010**;29:4959–70.

S22. Weisz B, Giehl K, Gana-Weisz M, Egozi Y, Ben-Baruch G, Marciano D, *et al*. A new functional Ras antagonist inhibits human pancreatic tumor growth in nude mice. *Oncogene* **1999**;18:2579-88.

S23. Zimmermann G, Papke B, Ismail S, Vartak N, Chandra A, Hoffmann M, *et al*. Small molecule inhibition of the KRAS-PDEδ interaction impairs oncogenic KRAS signalling. *Nature* **2013**;497:638–42.

S24. Shaw AT, Winslow MM, Magendantz M, Ouyang C, Dowdle J, Subramanian A, *et al*. Selective killing of K-ras mutant cancer cells by small molecule inducers of oxidative stress. *Proc Natl Acad Sci U S A* **2011**;108:8773-8.

S25. Papke B, Murarka S, Vogel HA, Martín-Gago P, Kovacevic M, Truxius DC, *et al*. Identification of pyrazolopyridazinones as PDEδ inhibitors. *Nat Commun* **2016**;7:11360.